CAPACITIVE STRAIN SENSORS FOR MEASUREMENT OF LARGE STRAIN

FOR STRUCTURAL HEALTH MONITORING

by

CLEMENT JACOB

Presented to the Faculty of the Graduate School of

The University of Texas at Arlington in Partial Fulfillment

of the Requirements

for the Degree of

MASTER OF SCIENCE IN ELECTRICAL ENGINEERING

THE UNIVERSITY OF TEXAS AT ARLINGTON

December 2010

ACKNOWLEDGEMENTS

ABSTRACT

CAPACITIVE STRAIN SENSORS FOR MEASUREMENT OF LARGE STRAIN

FOR STRUCTURAL HEALTH MONITORING

Clement Jacob, M.S

The University of Texas at Arlington, 2010

Supervising Professor: Donald Butler

Structural health monitoring (SHM) is increasingly used to replace time based management, with a more efficient Condition Based Maintenance (CBM). The traditional scheme of scheduling down time for aircraft inspection or periodic evaluation of civil infrastructure costs millions of dollars in maintenance due to either downtime or lack of timely maintenance. SHM involves periodic, real time sampling and analysis of signals, from onboard sensors like accelerometer, pressure, strain or acoustic sensors to determine the condition of the structure. This can be used to carry out immediate repairs as well as predict failure.

We report the development of a new high sensitivity capacitive strain sensor which can measure large strains. This can be used to measure large strains to detect failure as well as small variations to efficiently analyze and predict failure. Two different topologies are explored. The first comb based structure is a modification of a previously reported structure used for

measuring small strains. Despite the high sensitivity achieved, this topology suffers from some intrinsic limitations. This is addressed by the second parallel plate based topology. This retains advantages of the comb topology like high sensitivity and differential gain while overcoming limitations of maximum strain and also simplifies fabrication. A simple design approach has been used to realize both devices. Approximate equations are first used to establish course guideline for the design and then finite element method (FEM) based simulation is performed in CoventorWare$^{©}$ to optimize the devices. Several devices are designed in both topologies and optimum designs are selected from these. Since the device material will be subjected to large strains the material selection and fabrication process is developed simultaneously with the design. Considering readout requirements all sensors were designed for rest capacitance between 0.5pF to 1pF. The dimensions of the plate sensor, measuring similar strain (2%), were almost 60% smaller at 1500µm X 950µm as compared to the comb structure at 2450µm X 1350µm. The comb based topology demonstrated higher sensitivity with a gauge facto of 81 for 1% strain sensor and 51 for the 2% strain sensor, but could not be designed to measure higher strains. The plate structure had a gauge factor of 57, 38, 38 and 19 for 0.5%, 1%, 2% and 3% strain sensors respectively. A fabrication process is also outlined with emphasis on design specific requirements. In case of fabrication he plate structure would require a nominal aspect ratio of 2 as compared to 10 in case of the comb structure.

TABLE OF CONTENTS

LIST OF ILLUSTRATIONS

x

LIST OF TABLES

CHAPTER 1

INTRODUCTION

1.1 Overview

Structural health monitoring, (SHM) refers to the monitoring of various parameters like temperature, strain, acceleration, pressure etc. and analyzing it to detect damages to the structure. Traditionally, the maintenance of aircraft, ships, bridges and buildings is carried out by periodic evaluation of the structure using non-destructive evaluation techniques and visual observation. However increasingly, condition based, as opposed to time based maintenance is being explored. Condition based maintenance can potentially result in significant improvement in safety and save millions of dollars in maintenance cost.

1.2 Benefits of SHM

Aircraft are highly complex systems which are safety critical. Considerable monitoring of aircrafts is still done offline. It is estimated that a SHM system can save up to 44% inspection time [1]. There are more than 60,000 bridges in the United States which are inspected at least once every two years. According to a sufficiency rating around 40% are either structurally deficient or functionally obsolete [2]. Economic considerations do not make it feasible to upgrade the bridge infrastructure rapidly. A real time structural health monitoring system will enable constant monitoring of these structures, to avert potential disasters and plan a gradual redevelopment. Monitoring of buildings immediately after a natural disaster like an earthquake or hurricane using a real time structural health monitoring system will enable rapid evaluation of bridges, offices and buildings resulting in prompt availability of transport infrastructure and residential and commercial properties for re-occupation. This will help minimize the economic impact of such disasters [3]. Production lines can use SHM to diagnose potential equipment failure and carry out preventive maintenance to reduce downtime. This will also help optimize

1

the need of redundant machinery, to ensure continuous production in case of equipment failure[3]. This can again save millions of dollars in revenue. Another likely application for structural health monitoring is in equipment leasing. Equipment leasers of heavy construction machineries or jet engines can implement structural health monitoring and switch from time based leasing to condition based leasing. The user can be charged based on the system life used up, by implementing real time life cycle monitoring of equipment[4].

1.3 Current Applications of SHM

The most successful application of structural health monitoring has been in the damage diagnosis in rotating machinery. Essentially accelerometers are placed at strategic locations like the shaft of the motor and the vibration of the motor is monitored. The signal thus obtained is then compared with a database of signals obtained from the motor under different conditions. The correlation is then used to diagnose likely problems. Problems like damaged bearings or misaligned shafts can be diagnosed in this manner [5, 6]. NASA has developed the shuttle modal inspection system (SMIS) based on modal analysis, to detect fatigue damage to control surfaces, fuselage panels etc. where thermal insulating panels prevent usage of traditional NDE techniques [7, 8]. The US navy uses an integrated condition assessment system, in naval ships to monitor damages in its systems [9]. All these techniques rely on comparing the real time signal with a database of signals. A number of practical problems have prevented the widespread application of these techniques. An extensive and time consuming characterization is required to build the baseline databases. This might not be feasible, as a generic system is exposed to different climatic conditions, change in mass, temperature, pressure, wear and tear, machine noise etc. which will occur in an uncontrolled environment. A classic example of this issue was the failure to apply this technology to oil rigs in the 1980's.

A possible approach to account for this problem is to simply increase the data available to the diagnostic software. Instead of relying on a single variable like the vibration signature obtained from the accelerometer several sensors can be integrated in the SHM infrastructure. Different

2

sensors like pressure sensor, accelerometer, gyroscope, temperature sensor and strain sensor can be deployed simultaneously to monitor the structure. This data will enable a better diagnosis of the problem.

<u>1.4 Common Strain Sensors in SHM</u>

The most widely used strain sensors in structural health monitoring are metal foil sensors, semiconductor based piezoresistive strain sensors, and optical strain sensors.

1.4.1 Metallic Foil and Piezoresistive Strain Gauge

A metallic foil gauge strain sensor exploits the principle that the resistance of a metal piece changes due to deformation. It was first reported by Lord Kelvin[10]. Consider a metal block of resistivity ρ, length L, width W and height H. The cross sectional area A is the product of the width and height. The electrical resistance of the block is given as

$$R = \rho \, \frac{L}{A} \tag{1.1}$$

A strain induced deformation will cause a change in resistance given as

$$dR = \rho \frac{dL}{A} - \rho \frac{L dA}{A^2} + L \frac{d\rho}{A}$$

Dividing both sides by R

$$\frac{dR}{R} = \frac{dL}{L} - \frac{dA}{A} + \frac{d\rho}{\rho}$$

Now from definition of strain,

$$\frac{dL}{L} = \epsilon_L$$

And it can be shown that,

3

$$\frac{dA}{A} = -2v\epsilon_L$$

Where v is the Poisson's ratio. We can then reduce the above equation to,

$$\frac{dR}{R} = (1 + 2v)\epsilon_L + \frac{d\rho}{\rho} \qquad (1.2)$$

The first term gives the change in resistance due to geometrical variation of the resistor while the second term represents change in resistance due to piezoresistive effect. When the resistor is strained the distance between the atoms is increased. This results in a change in the band gap and a corresponding change in the curvature of the band edge. Therefore, the effective mass will change and this leads to a change in the effective carrier mass. Hence the mobility and the resistivity of the material will change. For metals, this effect is small as the bands are half-filled and small changes in the band gap or the band edges have no effect on the effective mass of the conduction electrons. For semiconductors, however, this effect can be quite large as there are fewer carriers in the conduction or valence band and these carriers will feel the change in the band structure. In effect, this leads to a change in the resistivity due to the applied stress.

$$\frac{d\rho}{\rho} = constant * \epsilon_L$$

$$\frac{d\rho}{\rho} = \pi_L E \epsilon_L$$

$$\frac{dR}{R} = (1 + 2v)\epsilon_L + \pi_L E \epsilon_L$$

$$\frac{dR}{R} = K \epsilon_L$$

$$K = (1 + 2v) + \pi_L E \qquad (1.3)$$

Where, K is the gauge factor. For metals π_L is quite small and the gauge factor is approximately given by

$$K \approx (1 + 2v) \approx 1.5 \ to \ 2$$

4

In case of semiconductors $\pi_L E$ can be quite large and gauge factor can vary from 10 to 150. However this is highly dependent on the doping and varies widely with temperature. The piezoresitive coefficient π_L can be written in terms of a temperature T and doping N dependent factor P(N, T) as

$$\pi_L = P(N,t)^* \pi_L(300K) \qquad (1.4)$$

The scaling factor has been reported by Kanda et al [11]. As the concentration of the majority charge carrier increases from 10E16 atoms/cm^3 to 10E20 atoms/cm^3 the scaling factor varies from 1.5 to 0.2 for p-type Silicon and 1.5 to 0.4 for a n-type silicon. This results in a large variation in gauge factor of semiconductor based strain sensors with temperature. The resolution of a resistive sensor is limited by the thermal noise associated with the active element. It is given as

$$V_{Thermal} = \sqrt{4k_B TRB} \qquad (1.5)$$

Piezoresistors are good for operation in controlled environment. Metal Strain Gauges generally have a relatively low gauge factor. While novel techniques have been employed to increase gauge factor of metal film strain sensors, these are either sensitive to temperature or lack stability[12, 13]. Semiconductor based piezoresistive sensors show high dependence on temperature[14, 15], and are susceptible to electrical noise. Carbon nanotube based strain sensors show high dynamic range and sensitivity but its' gauge factor is prone to temperature variation[16, 17], making it unsuitable for applications that require wide operating temperature. The use of MEMS piezoresitive sensors is generally limited to applications which involve small strains.

1.4.2 Fiber Optic Strain Sensors

Fiber optic strain sensors are one the most popular strain sensors used for structural health monitoring. As opposed to electronics based system optical sensors offer several advantages. They are intrinsically free of electromagnetic parasites, high pressure and ionizing radiation. It is

extremely sensitive and a single fiber can be used in multiplexed configuration to deploy a distributed sensing system.

The optical strain sensors can be broadly classified as intensity based system, phase shift based system and frequency based system. Intensity based system is the simplest optical strain sensor. It uses the principle that a multi-mode optical fiber exhibits a decrease in transmissibility with an increase in applied strain. However it is difficult to differentiate between reduction of intensity due to strain and reduction due to losses at connectors, fiber damage and fluctuations at source power levels.

Phased based optical strain sensors using interferometry is another popular strain measurement technique. It typically involves splitting a coherent source into two beams. The optical path off one of the beams is exposed to the strain, which induces a phase shift in the signal. The two beams are then combined to generate an interference pattern. The Fabry-Perot sensor is an interferometer based strain sensor. The sensor consists of two pieces of optical fibers separated by an air gap. The end of the fiber has a metal layer evaporated on it so that it acts like partial mirrors. The light transmitting in the fiber is partially reflected by the first mirror, the remaining light is transmitted through the first mirror, through the air gap and is again partially reflected by the second mirror. The two reflected light waves combine to form an interference pattern. This number of fringes N, passing a given point is proportional to the applied strain and is given as

$$N = \frac{\delta\Phi}{2*\pi} = \frac{\epsilon \, X \, l}{\lambda(n+1)} \tag{1.6}$$

Where, $\delta\Phi$ is the phase shift in the light wave of wavelength λ, due to a strain ϵ, in a fiber of length l and refractive index n. Michelson-Morley interferometer and Mach-Zehnder interferometer based strain sensors have similar operating principles. The fiber Bragg grating based strain sensors have a grating pattern written on the inner core using holographic

6

techniques by side exposure of a UV light interference pattern. The transmitted frequency is given as

$$\lambda_B = 2n\Lambda \qquad (1.7)$$

Where, n is the refractive index of the core and Λ is the period of axial variation in n. A change in strain changes the Bragg wavelength as

$$\lambda_b(\epsilon, t) = \lambda_B(\epsilon_o, T_o) + S_\epsilon(\epsilon - \epsilon_o) \qquad (1.8)$$

Where, S_ϵ is the strain sensitivity to wavelength. An advantage of grating based optical strain sensor is that many gratings can be written on a single optical fiber, so as to get a distributed strain sensor.

Despite the many advantages of optical strain sensors there are certain limitations to this sensor. A sharp bend will cause significant signal loss which will affect the reading. So it cannot be used as a truly conformal sensor. Also temperature variation will cause expansion or contraction of the optical fiber and this will be difficult to differentiate between strain induced and temperature induced signal variations. Also any breakage of the fiber at either the input/output ports or through the length of the fiber will result in failure of the entire distributed array of sensor on the fiber. Also optical techniques require complex signal analysis. In case of interferometer sensors the signals have to be analyzed by a computer which will consume power and time especially for a large array of sensors. A fiber Bragg sensor will require a spectrometer[18].

<p align="center">1.5 Capacitive Strain Sensors</p>

Capacitive strain sensors have been employed since the early 90's due to distinct advantages over conventional metal foil strain sensors. The advances in capacitive strain sensors and MEMS fabrication technology prompted the development of MEMS based capacitive strain sensors. Ko et. al. developed a buckled beam strain sensor with a comb structure[19]. It used

<p align="center">7</p>

buckled beam amplification as well as an array of combs to achieve high sensitivity. Lin et. al. used a simple cantilever based system to form an air gap capacitor[20]. The device achieves a high gauge factor at the expense of large device dimensions (7mm X 2mm) and a complex readout circuitry however it is suitable for measuring only small strains. A thick film based capacitive sensor was reported by Arshak et al [21] that used a lead zirconate titanate (PZT) or polyvinylidene fluoride (PVDF) dielectric, sandwiched between two metal electrodes. This structure however restricts plate motion and hence results in a low gauge factor. Que et. al. developed a buckled beam capacitive strain sensor [22] but the maximum measured strain reported was around 0.03% . A capacitive strain sensor has been developed for measuring large strain by Matsuzaki and Todoroki [23]uses a lateral or a transverse patterned electrode on epoxy resin substrates. While it can measure large strain, sensitivity is very small beyond a few thousand micro strains. The capacitive strain sensors developed by different groups is summarized in Table 1.1

Table 1.1 Brief Overview of Some Reported MEMS Strain Sensors

Group	Type	Flexible	Maximum Strain	Gauge Factor
Ko et al	Capacitive Buckled Beam	No	0.10%	-
Lin et al	Capacitive Cantilever Air Gap	Yes	0.10%	249
Arshak et al	Capacitive sandwiched dielectric membrane	No	-	3.5
L. Que et al	Capacitive Buckled Beam	No	0.03%	-
Matsuzaki and Todoroki	Capacitive in plane patterned electrode	Yes	~3%	-

1.6 Goals

The strain sensor should be able to meet the following requirements. It should be flexible to enable it to conformally comply with different structures. It should be able to measure very large strains in order to diagnose large deformations, delaminating repair patches and cracks, but at

the same time it should have high gauge factor to detect small variations in the strain for real time monitoring. The strain measurements should be independent of temperature to enable measurement over a wide temperature range.

The objective of this research was to develop a strain sensor that meets the following criteria's.

1) It should have minimum impact on strain distribution in the structure

2) It should be conformal on the surface where strain has to be measured

3) It should transfer all the strain on the surface to the transducer mechanism

4) It should have high sensitivity, dynamic range, bandwidth and be capable of measuring large strain up to 3%.

5) It should be reasonably insensitive to ambient factors like temperature and pressure.

6) It should be inexpensive to fabricate, install and operate

1.7 Thesis Organization

Chapter two describes the basics of stress and strain and introduces fundamental concepts involved. Chapter three describes the actual design. It starts with material selection, compares possible materials that can be used and gives the rationale behind the choice of materials. The theory of the design and its operation is covered in detail. Standard design equations are used to realize a coarse design which is later optimized using FEM analysis. Chapter four gives the design and analysis of the sensor using FEM simulation. The physics of simulation and its application to this design is briefly described along with the design. Chapter five gives a detailed fabrication process outline for the sensor. Detailed analysis of available material and equipment options is presented and choice of fabrication steps and material is justified. Chapter six summarizes the design goals achieved, compares the two sensor topology and conclusions drawn are presented. Recommendations for further research are also given.

CHAPTER 2

STRESS AND STRAIN

Stress and strain in the device is one of the most fundamental criteria for ensuring proper device operation. In this design, it is interestingly not only the quantity to be measured but also the biggest limitation on the device.

2.1 Stress

Stress is effect on a cross section of interest. The force on the cross section can be resolved into defined as force per unit area. The effect of force on a structure is analyzed by observing its components perpendicular and parallel to the section. Consider a small element, with ZY face being the section of interest. The force F on the elemental surface of area ΔA can be resolved along X, Y, and Z direction as ΔF_x, ΔF_y and ΔF_z. The stress on the surface can then be given as

$$\sigma_{xx} = \lim_{\Delta A \to 0} \frac{\Delta F_x}{\Delta A} \qquad \sigma_{xy} = \lim_{\Delta A \to 0} \frac{\Delta F_y}{\Delta A} \qquad \sigma_{xz} = \lim_{\Delta A \to 0} \frac{\Delta F_z}{\Delta A} \qquad (2.1)$$

The first subscript indicates that the plane perpendicular to the X axis is considered and the second designates the direction of the stress. The force per unit area perpendicular to the surface is called normal stress. σ_{xx}, σ_{yy} , σ_{zz} are normal stresses. Normal stress that causes tension is called tensile stress while it is called compressive stress if the stress pushes against the surface. Stress acting parallel to the surface is called shear stress. σ_{xy}, σ_{yz} ,σ_{zx} etc. are shear stress acting along the faces. The units commonly used for stress are Pascal, Newton/m^2, dynes/cm^2, pound/inch^2 (psi). These units can be converted into one another by using the approximate relation, 1 atm ~ 14 psi ~ 100 KPascal ~ 760 Torr ~10 dynes/cm$^{2.}$
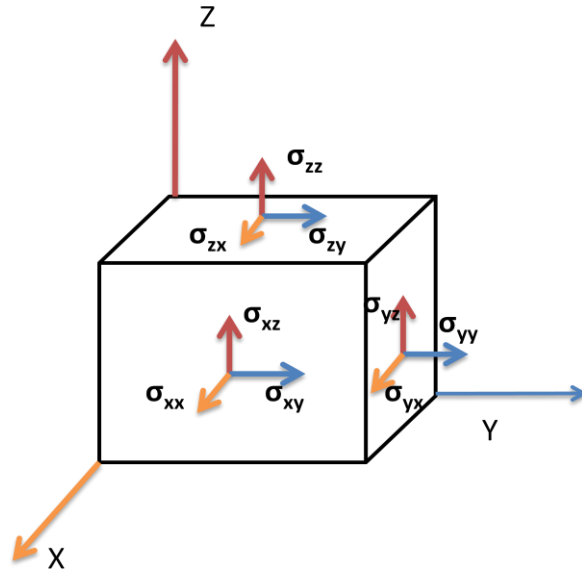
Figure 2.1 Elemental Block Indicating the Different Stress Components

2.2 Strain

When stress is applied to a body it deforms. The differential deformation is called strain. Normal or uniaxial strain ε_x, ε_y, ε_z is the ratio of change in length in corresponding direction to the original length. Shear strain γ_{xy}, γ_{yz}, γ_{zx} etc measure the moving of plates over each other with the subscripts following the same convention as in stress. Strain is a unit less quantity and generally expressed in micro strain. One micro strain is same as one part per million (ppm) deformations.

In general, mechanical modeling involves finding the relationship between stress and strain. The stress strain curve is frequently used to characterize material behavior. The stress strain curve for different materials can vary greatly depending on their properties. A generic stress strain curve is given in figure 2.2. Initially for small stress most materials obey Hooke's law and stress is linearly proportional to strain. This behavior is consistent up to the proportionality limit. When a stress corresponding to the yield strength develops in the structure, the material begins to deform irreversibly. Beyond the yield point, the molecular structure of the material changes so

11

as to attain a new equilibrium arrangement. This rearrangement results in permanent deformation of the structure.
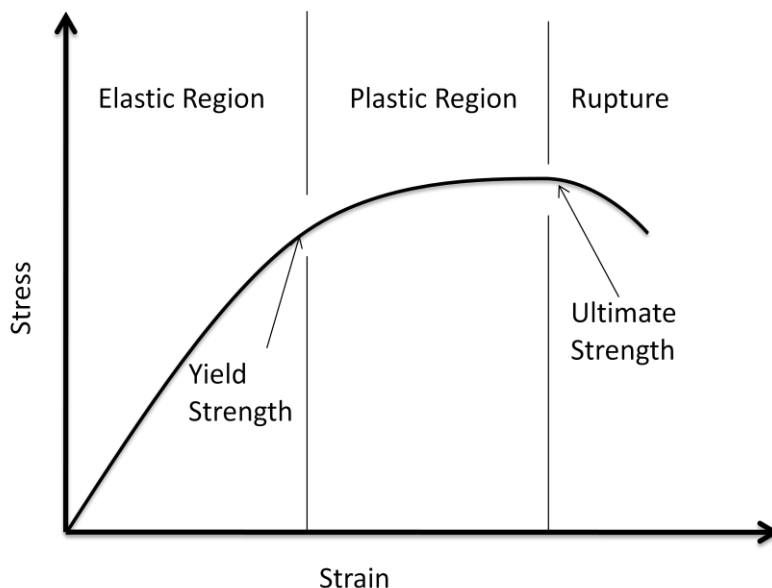
Figure 2.2 Generic Stress Strain Curve

In case of a crystalline material, the rearrangement occurs due to dislocation motion. However if the material micro-structure does not allow dislocation motion, which occurs in case of brittle materials, it simply fractures. Ductile materials continue to deform in the plastic region with a small change in stress corresponding to a large change in strain. In polymers the elastic properties depend on the arrangement polymer chains i.e. orientation and also crystalline nature. It can display brittle, yielding or rubber-like behavior[24, 25]. Polyimide behaves like a ductile material. The true stress is not uniform throughout the surface and the local stress at a defect site is much higher than average. The cross sectional area at this point starts reducing resulting in necking and all further plastic deformation is concentrated at this point. Ultimate tensile strength is the maximum stress that a material can withstand before necking is initiated. Ultimate strength is commonly used for brittle materials which fail while still in the linear region and do not have a yield point. Once necking initiates in

ductile materials, the stress reduces but strain continues to increase and eventually results in a fracture.

Stress is primarily analyzed to predict device failure. Depending on the loading conditions, material properties and critical nature of the device a variety of failure theories can be utilized for design. The loading can be either static or fluctuating for either ductile or brittle material. Also a large safety factor is maintained in very critical application as compared to devices for nominal usage. Materials that elongate more than 5% before failure are called ductile material. In case of a ductile material, if the stress exceeds the yield strength of the material then a permanent deformation results.

<u>2.3 Tresca and Von Mises-Hencky Stress</u>

The Tresca or maximum shear stress theory and the Von Mises- Hencky or distortion energy theory are most commonly used failure theories for ductile materials under static load.

The maximum shear stress theory states that ductile materials fail due to slippage of crystal planes due to shear stress. The failure is most likely to occur due to shear stress as the yield strength in shear is roughly half that of the yield strength in tension or compression. Thus for failure,

$$\tau_{max} \geq \frac{S_y}{2} \tag{2.2}$$

S_y is the yield strength of the material. It thus states that the shear stress should not exceed half the yield strength. The distortion energy theory postulates that the shear strain energy rather than shear stress gives a more accurate insight into material failure. Strain energy is the energy stored within the body when its shape or volume is distorted within the elastic zone. The Von Misses criteria states that the material failure occurs when the strain energy in the body per unit volume exceeds the strain energy in the same volume when stress in it equals uni-axial yield stress. It uses an effective stress, known as von mises stress, to determine failure. Von Mises stress (σ') is the tensile stress that would cause the equivalent distortion energy as created by the actual stress.

13

$$\sigma' = \sqrt{\frac{(\sigma_1 - \sigma_2)^2 + (\sigma_2 - \sigma_3)^2 + (\sigma_3 - \sigma_1)^2}{2}} \tag{2.3}$$

Where σ_1, σ_2, σ_3 are the principal stresses. The principal stresses are the maximum stresses for any orientation of the element. Failure occurs when

$$\sigma' \geq S_y$$

While both theories are acceptable and give similar results the tresca theory is more conservative and relatively easier to compute.

In case of brittle materials like polysilicon or silicon nitride, maximum principal stress theory, Coulomb-Mohr theory and modified Mohr theory is commonly employed. It is important to remember that unlike ductile materials, brittle materials have different strengths in tension and compression. The maximum principal stress theory states that failure will occur when the maximum principal stress exceeds the ultimate uniaxial tensile/compressive stress of the material. The maximum principal stress is given by the larger of the two values given by,

$$\sigma_{max} = \frac{\sigma_x + \sigma_y}{2} \pm \sqrt{\tau_{xy}^2 + (\frac{\sigma_x - \sigma_x}{2})^2} \tag{2.4}$$

Failure occurs when σ_{max} exceeds the ultimate tensile/compressive strength of the material[26].

2.4 Safety Factor

A convenient form to apply both Coulomb-Mohr theory and modified Mohr theory uses a variable denoted as safety factor (SF). The safety factor should always be greater than 1 to avoid device failure. The Coulomb-Mohr theory gives the safety factor as

$$SF = \frac{S_{ut}}{\sigma_1} \ \ when \ \sigma_1 \geq 0 \ and \ \sigma_1 > \sigma_3 \tag{2.5}$$

$$SF = \frac{S_{ut}S_{uc}}{S_{uc}\sigma_1 - S_{ut}\sigma_3} \ \ when \ \sigma_1 \geq 0 \ and \ \sigma_3 < 0$$

14

The modified Mohr theory gives the safety factor as

$$SF = \frac{S_{ut}}{\sigma_1} \ \ when \ \sigma_3 \geq -S_{ut} \tag{2.6}$$

$$SF = \frac{S_{ut}S_{uc}}{S_{uc}\sigma_1 - S_{ut}(\sigma_1 + \sigma_3)} \ \ when \ \sigma_3 < -S_{ut} \tag{2.7}$$

While both theories give acceptable failure criteria the Coulomb-Mohr theory is more conservative.

CHAPTER 3

SENSOR DESIGN

The proposed design uses the principle of compliant design instead of traditional rigid link design. The former is especially popular in MEMS design as it simplifies fabrication – translating to lower costs and improves device reliability – by reducing wear, increasing precision and minimizing number of parts in the device. Common appliances that exploit compliant mechanism include tweezers, paper clip or nail cutters. However compliant mechanism present several unique challenges. The complaint structure is often subjected to large deflection, which cannot be characterized by linear beam equations. The material selected should have both strength and flexibility.

Two design approaches are pursued in this work. The first approach uses a comb based buckled beam structure, which has been successfully used to measure small strains up to 1000με earlier. An alternate design method was used as the approximations used for designing a sensor, for measuring small strains, is not valid for large deflection device. However despite the new design methodology developed, the basic topology of this sensor has intrinsic limitations on fabrication and range of operation. An alternate plate based design was developed to address these issues. At the same time advantages of the previous structure like mechanical amplification and differential measurements were incorporated in the new design. The device mechanism and underlying theory is presented in this chapter.

3.1 Device Operation

3.1.1 Capacitive Comb Based Sensor

The capacitive comb based structure is shown in figure 3.1 below. The strain applied to the structure along the X axis, causes the arms to move in the Y direction. The net displacement of the arms can be enhanced by appropriately designing the length and angle of the arms. The

16

two outer electrodes move in the positive Y direction, while the central electrode moves in the opposite direction. This increases the overlap area and hence capacitance, between the lower pair of combs and reduces the overlap area and capacitance between the upper pair. This double differential mechanism further increases the sensitivity of the sensor. However this design limits the maximum measureable strain. The capacitance is inversely proportional to the gap between the comb fingers and the length of the fingers. If strain is applied in a direction perpendicular to the fingers, ideally both combs should move parallel to each other. However there will always be components of strain in other directions as well. This will result in a slight angle between different comb sets. Long arm and finger lengths will further aggravate this problem. This places a severe limitation on both the allowable gap between the fingers and the length of the fingers, thus reducing capacitance and sensitivity of the device. Another method to increase capacitance and hence sensitivity is to increase the height of the fingers to increase the plate area of the capacitors. However this will result in a sharp increase in the aspect ratio of the device, which will result in tougher constrains on fabrication, potentially making the sensor more expensive. The maximum measurable strain is limited by the length of the fingers and the required finger overlap area. At the limiting strain, the fingers of adjacent comb will touch the support beam or there will be no overlap area between adjacent combs. This is an intrinsic limitation of this design. An alternate design, a plate based structure has been proposed to address these issues.
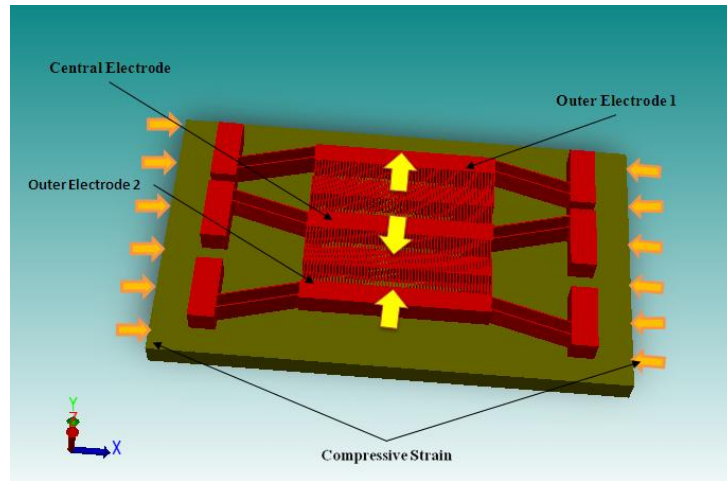
Figure 3.1 Basic Structure of the Capacitive Comb Strain Sensor

3.1.2 Capacitive Plate Based Sensor

In the plate based structure (figure 3.2), the top plate is suspended by four cantilever beams. Two electrically isolated metal patches are present directly below the suspended plate. There are two capacitors in this structure, one consists of   the top plate, the air gap acts as the dielectric and bottom electrode 1 is the second electrode. Similarly the second capacitor is formed between the top plate and bottom electrode 2. Strain applied to the structure along the length of the arms, i.e. in the X direction, displaces the plate in a perpendicular direction along the Y axis. The plate moves either forward or backward depending on the nature of the strain i.e. compressive or tensile and the angle of inclination of the arms. The strain induced motion results in an increase in the area of one capacitor and a proportional decrease in the area of the second capacitor. This gives a linear differential capacitive variation in response to the applied strain. The plate structure greatly relaxes the fabrication requirements of the design compared to comb structures.

18
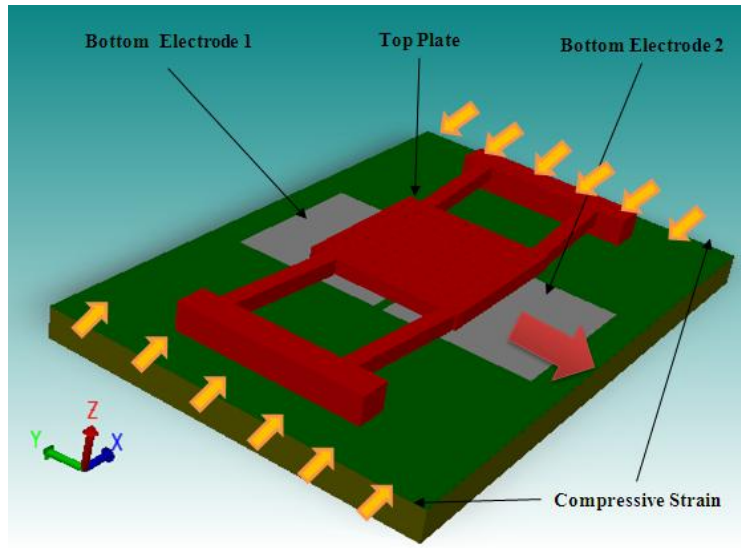
Figure 3.2 Basic Structure of the Capacitive Plate Strain Sensor.

3.2 Material Selection

Material selection was a critical part of the design. The criteria employed for the choice of materials include mechanical properties like strength and elasticity, electrical properties like conductivity and dielectric constants and material availability and fabrication ease.

3.2.1. Substrate Material

Traditionally silicon is used as a substrate for MEMS devices. However this limits its use to planar surfaces. Also the rigid nature of the material results in an inefficient transfer of strain from the substrate to the device. Since the sensor needs to be conformal a flexible substrate was required for this design. A wide range of polymers have been used as flexible substrate like parylene, PDMS, Polyimide etc based on the application[27]. Parylene and Polyimide are considered for this design.

3.2.1.1 Parylene

Parylene has been successfully used as a substrate[28, 29]. Parylene is a common generic name for a unique series of polymers based on paraxylene. The three most common types of parylene are referred to as: Parylene N, Parylene C, and Parylene D. In actual usage,

Parylene C is the most common type of parylene used for almost all types of applications. The basis for the parylene family is the polyp-xylene monomer which comprises Parylene N. Parylene C and D are created by the substitution of a single chlorine molecule (C) or two chlorine molecules (D). Parylene is applied at room temperature with specialized vacuum deposition equipment that permits control of coating rate and thickness. The deposition process takes place at the molecular level as the chemical, in dimer form, is converted under vacuum and heat to dimeric gas, pyrolized to cleave the dimer, and finally deposited as a clear polymer film. The films thickness can vary from few 100A^o to several micrometers.

(a) Parylene N   (b) Parylene C   (c) Parylene D
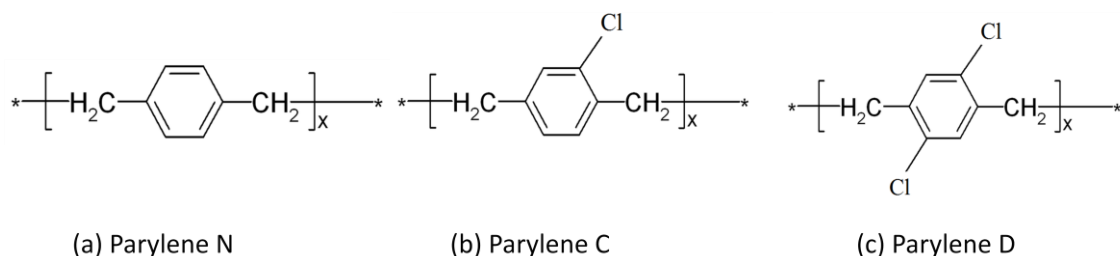
Figure 3.3 Chemical Structure of Parylene

3.2.1.2 Polyimide

Polyimide (PI) is a polymer of imide monomers. Based on the functional groups in the main chain, polyimides can be aliphatic, semi-aromatic or aromatic. Aromatic polyimides are the most popular due to its high thermal stability. Polyimides can be either thermoplastic (changes between solid and liquid state based on temperature) or thermosetting (i.e. irreversibly turns solid on curing). The latter is commercially available as uncured resins, polyimide solutions, or as sheets. Thermosetting polyimides are known for thermal stability, good chemical resistance, excellent mechanical properties, and characteristic orange/yellow color.
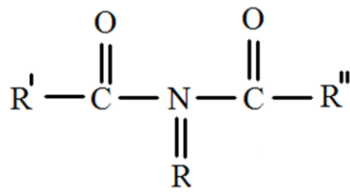
(a) General Polyimide Structure   (b) Aromatic Polyimide Structure
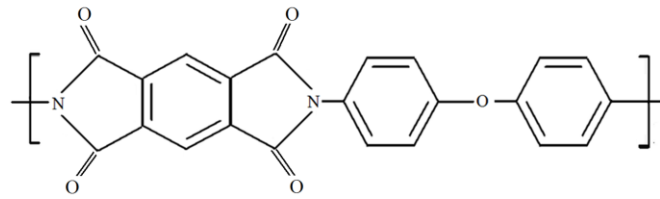
Figure 3.4 Chemical Structure of Polyimide

Parylene and polyimide are compared along with silicon in the table below. PI 2611 from HD Microsystems was selected due to its low Young's modulus, high tensile strength and low stress. It can be conveniently spin coated on a silicon wafer and cured at appropriate temperature to obtain the required substrate thickness.

Table 3.1 Material Properties for Different Substrates

Properties	Polyimide [30]	Parylene[31-33]	Silicon [34]
Young's Modulus	2.1 -8.1GPa	4.7GPa	155.8GPa
Poison's ratio	0.34	0.4	0.2152
Mass Density	1.42 gm/cm^3	1.289 gm/cm^3	2.32 gm/cm^3
Yield Strength	_	59MPa	_
Tensile Strength	260-350MPa	69MPa	3790MPa
Thermal Conductivity	0.12 W/m.K	0.082 W/m.K	149 W/m.K
Melting Temperature	Decomposes at 500°C	290 °C	1412° C
Coefficient of Thermal Expansion	3-30ppm/°C	3.5ppm/°C	2.6ppm/°C
Etch	O_2 Plasma Etch	O_2 Plasma Etch	Wet or dry etch
Dielectric constant	3.4	3.1	11.8

3.2.2 Structural Material

A conductive structural material is required for the plate electrode. Single crystal silicon, polysilicon and nickel are the most popular materials used in MEMS for this purpose. Amongst these polysilicon and nickel are attractive due to relatively simple fabrication methods.

3.2.2.1 Silicon

Single Crystal Silicon (SCS) is a continuous structure consisting of silicon atoms in a diamond lattice structure. Single crystal silicon is predominantly grown for making substrate wafer using Czochralski growth method or the float zone Method. Molecular Beam Epitaxy is also used to grow SCS. The high cost involved in the latter method makes it less attractive. Thermal oxidation of silicon depends on temperature and crystal plane. Anisotropic etch of Single Crystal Silicon can be done using either wet etchants like ethyline- diamine pyrocatecol (EDP) or potassium hydroxide (KOH). Dry etching techniques include reactive Ion etching (RIE) and reactive ion beam etching (RIBE). A mixture of HF, HNO^3 and water or acetic acid can be used to etch SCS in an isotropic manner. Single crystal silicon (<100>) has a young's modulus of 130GPa. Tensile strength of silicon is around 3.79GPa.

Polysilicon consists of many grain like structures separated by grain boundaries. The grains are self contained mini-crystals, whose orientation varies with respect to each other. The presence of grain boundaries in polysilicon introduces a variety of electrical and mechanical properties in polysilicon. LPCVD is the most popular method for depositing polysilicon films. The structure of the film depends on the temperature and film thickness. For a typical LPCVD process (100% SiH4 source gas, 200mTorr deposition pressure) the amorphous to polycrystalline transition occurs at around 570 degree Celsius [35]. Unlike SCS in polycrystalline silicon subsequent high temperature processing like doping thermal oxidation etc., will cause a change in orientation and grain size. The grain structure in polysilicon possesses a unique problem not seen in single crystal silicon. The rough surface due to its granular nature or grain growth due to heating in subsequent steps can cause problems in photolithography. Also the rough surface can act as an initiating point for structure failure. Chemical mechanical polishing can be used to minimize this. Wet etchants like KOH etch isotropically due to the grain structure of polysilicon. In case of polysilicon the young's modulus depends on crystal structure and orientation which is highly dependent on deposition conditions. It has been reported in the range of 140GPa to 210GPa. In

polycrystalline silicon the fracture strength depends on grain size and fracture surface energy. The energy needed to fracture a grain surface increase with grain size [34].

3.2.2.2 Nickel

Nickel is popular structural element in MEMS for its ease of fabrication. It can be used to make high aspect ratio structures using electrodeposition. Like polysilicon it also composed of many grains. It is possible to vary the mechanical properties of the structure by varying the grain size. This can be achieved easily by varying the current density during electrodeposition. It has been demonstrated that current density of 15mA/cm^2 gives a Young's modulus of 171GPa and yield strength of 450MPa and density of 2mA/cm^2 gives a Young's modulus of 204GPa and yield strength of 995MPa[36, 37]. This is particularly useful for structures subjected to large deflection. Also due to its conductive nature it is convenient to use it for electrical sensors.

The properties of SCS, polysilicon and Nickel are listed in table 3.2. Nickel is chosen as the structural material due to availability of fabrication setup and excellent mechanical and electrical properties.

Table 3.2 Material Properties for Structural Materials

Properties	Nickel	Polysilicon[38]	Single Crystal Silicon
Young's Modulus	200GPa	169GPa	155.8GPa
Poison's ratio	0.31	0.22	0.2152
Mass Density	8.9 gm/cm^3	2.33 g/cm^3	2.32 gm/cm^3
Yield Strength	450-995MPa	-	-
Tensile Strength		1.2GPa	3.79GPa
Thermal Conductivity	91 W/m. °K	148 W/m. °K	149 W/m. °K
Coefficient of Thermal Expansion	13ppm/°C	4.7ppm/°C	2.6ppm/°C

3.3 Device Design

The different design parameters like the inclination, length, width and thickness of the beam, plate size, gauge length, anchor size were determined based on required specifications of

sensitivity, dynamic range and limiting factor like yield stress, pull-in voltage, flexible substrate consideration and ease of fabrication. The flexible substrate is one of the key properties of this design. The polyimide substrate will ensure compliance with the surface as well as the maximum strain transfer from the test specimen to the sensor.

3.3.1 Capacitive Comb Based Sensor

The maximum deflection occurs in the y direction and this will determine the maximum stress in the device. The comb section can be assumed to be a point mass and deflection is expected to occur almost entirely due to beam deformation. The spring constant and maximum elastic deflection in the beam in the Y - direction is given by

$$K_{my} = \frac{Eb^3h}{l^3} \tag{3.1}$$

$$\delta_{max} = \frac{Sl^2}{6Eb} \tag{3.2}$$

Where, E is the Young's modulus, b is the beam width, h is the beam thickness, l is length of the arm, δ_{max} is maximum deflection in y direction and S is the yield stress of the material. The plate and beam structure will be electrodeposited nickel. Although reducing width from 10 μm to 5 μm doubles the maximum possible displacement, this reduces the spring constant by a factor of b^3. While a reasonable flexibility is required to get elastic deformation of the arms in the Y direction, the beams have to be stiff enough to translate the force applied due to the strain along X axis to a displacement along Y axis. The beam equation is for a free standing beam while the beams in the structure are guided ones. It is expected that if the beams have reasonable stiffness, the guided beam in the sensor and free beam would have similar maximum allowed displacement. While details of FEM simulation will be covered in the next chapter the FEM results are given here for comparison. The FEM result confirmed the expected correlation between the two.

24

Table 3.3 Displacement Corresponding to Yield Stress in Simple Cantilever (Theoretical) and in an Arm of the Sensor obtained from FEM

Design Parameter		E=170GPa,S=450MPa	E=200GPa,S=990MPa	FEM Analysis for E=200GPa,S=990
l(μm)	b(μm)			
600	5	31.75	59.4	19
700	5	43.23	80.85	13.6
700	10	21.62	40.425	56
800	5	56.47	105.6	14
800	10	28.24	52.8	64

The comb structure is particularly susceptible to substrate deformation in case of a flexible substrate. The adjacent set of combs is independent of each other and deformation can cause misalignment between them. The maximum gauge length was set to 2.5mm accounting for the flexible substrate, topology requirement and desired electrical properties. Since the device is intended to measure high strains, and also considering fabrication aspects like adhesion of anchor material to the polyimide substrate, 150μm X 200μm X 20μm anchors were used. Devices have been designed and optimized for different dynamic range and sensitivity.

Combs have 40 to 60 fingers, with each measuring 240μm x 7μm x 20 μm and 160μm x 5μm x 20μm respectively. The gap between the fingers of adjacent electrodes varies from 2 μm to 3 μm. The rest capacitance of the sensors varies between 550fF to 1000fF. Sensors were designed to measure strains up to 1% and 2%. Higher strain measurements would require larger comb dimensions and the device size becomes unfeasible for implementation on a flexible substrate.

3.3.2 Capacitive Plate Based Sensor

The displacement considerations of the plate based sensor are similar to that of the comb structure. The plate structure arm is designed to optimize stress as was done in the comb structure. A unique limitation for the plate design is the pull-in phenomenon. The device will be

operated at around 2.5V and a pull-in voltage of at least 10V is required. The pull-in voltage is again decided by the spring constant of the structure in the Z direction. The spring constant in Z direction K_{mz} and the pull-in voltage $V_{pull-in}$ are given as

$$K_{mz} = \frac{4Eh^3b}{l^3} \tag{3.3}$$

$$V_{pull-in} = \frac{2d}{3}\sqrt{\frac{K_m}{1.5C}} \tag{3.4}$$

Where d is the separation between the plates and C is the capacitance of the structure. Since the beam length and beam width is fixed by stress constrains the beam thickness and plate separation will be used to meet the minimum pull-in requirement. The capacitance value and approximate beam dimensions obtained earlier was used to validate initial values give tolerable pull in voltages.

While a capacitive sensor intrinsically requires large area to maximize capacitance, small dimensions will make it more robust and easier to integrate with associated electronics. The design structure was modified so as to make it more compact, while maintaining all the above design parameters (Figure 3.5). The sensor length is reduced by almost 700 μm. The initial plate dimension was 500 μm X 500 μm. Slots are cut into the plate for this purpose, such that the rest capacitance reduces but sensitivity remains unchanged. This can be easily ensured once the maximum allowable deflection is decided. Likewise slots are cut in the anchor allowing appropriate clearance for beam deflection. The mechanical gain of the design needs to be optimized for linearity and dynamic range. A strain applied in the X direction causes the arms to propel the plate in a perpendicular direction. The gain improves the sensitivity but the corresponding amplification in the plate deflection increases the stress in the beam.
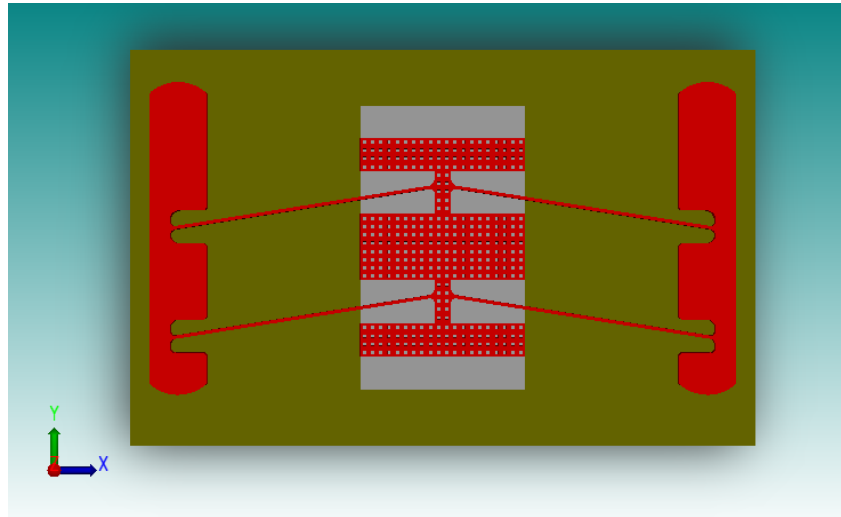
Figure 3.5 Modified Compact Version of the Sensor

CHAPTER 4

SIMULATION

4.1 Introduction

Mechanical or electrical systems are analyzed by modeling the system using differential equations, which relates the different variables of the system using fundamental laws like conservation of energy, conservation of mass, laws of thermodynamics, Maxwell's equation, and Newton's law of motion. The solution is then obtained by either eliminating the differential equation completely by converting them into steady state equation, or rendering the partial differential equations into an approximating system of ordinary differential equation which can be numerically integrated using standard techniques. However these equations are difficult to solve specially for complex geometrical shapes and non-linear phenomenon. It is difficult to formulate sufficiently accurate equations that approximate the equation to be studied, which is numerically stable, i.e. errors in the input and intermediate calculations do not accumulate and cause the resulting output to be meaningless. Several techniques have been developed to simplify the computation. These include finite difference technique, weighted residual methods, variational method and finite element analysis. The finite difference method approximates the derivatives in the differential equation using difference equations. It is useful for solving heat transfer and fluid mechanics problems. It works well for two-dimensional regions with boundaries parallel to the coordinate axes. However it is difficult to tackle regions with curved boundaries. The weighted residual method tries to satisfy the differential equation in an average sense by converting it into an integral equation. The differential equation is multiplied by a weighting function and then averaged over the domain. The different techniques used include collocation, subdomain, least squares and galerkin's method. Variational methods, least square and galerkin's methods are also used in finite element method.

The finite element method (FEM) utilizes nodal location, elements connecting the nodal points, mass properties, boundary conditions, loading function details and analysis options as input. A FEM software first divides the structure into elements. While the original structure has infinite number of degrees-of-freedom (DOF), the discretized model has a finite number of DOF. The individual elements are then linked at the nodes and the effects of loads and boundary conditions are used to obtain a set of linear or nonlinear algebraic equations. The solution of these equations gives the approximate behavior of the continuum or system. Depending on the type of system equations obtained different techniques are employed to find the solution. In case of differential equation, then the most popular solution method is the method of weighted residuals. In numerical optimization problems (minimization of function) variational formulation is employed. In the MWR, an *approximate* solution is substituted into the differential equation. Since the approximate solution does not identically satisfy the equation, a residual, or error term, results. Galerkin's method is popularly used to find the weighting function. The variational method involves the integral of a function that produces a number. Each new function produces a new number. The function that produces the lowest number satisfies the differential equation. Several FEM analysis tools are commercially available. These include ANSYS, CoventorWare, COMSOL, and ABAQUS. We have used CoventorWare for design optimization.

4.2 Need for Simulation

While the concept of buckled beam has been used for mechanically amplified strain sensor it has only been demonstrated to measure up to 1000uɛ. We intend to extend this method for measurement of strains up to 25000uɛ. The double beam structure for the comb is being attempted for the first time. The plate structure for buckled beam strain measurements is also never reported before. Large strain measurements involve unusually large deflection. Simulation was initially used to establish feasibility of these designs. Once this was established the designs were optimized and tested for different specification using design the guidelines

29

developed in the previous chapter. The simulation and analysis of the structures for mechanical characterization was done in CoventorWare's MemMech module.

<u>4.3 Mechanical Simulation</u>

The MemMech module primarily calculates stress and displacement. The material property database is used to set the mechanical and electrical properties of the materials used for the device. The material properties used for the different materials in both the comb and plate structure simulation is listed in the table 4.1 below.

Table 4.1 Material Properties Used for MemMech Simulation

	Nickel	Polyimide	Silicon Nitride
Modulus of Elasticity	170MPa-220MPa	7500MPa	220MPa
Poisson's Ratio	0.3	0.35	0.27
Density	8.91E-15 kg/μm^3	1E-15 kg/μm^3	2.7E-15 kg/μm^3

Appropriate layouts were designed in Designer and representative models of both the capacitive plate structure and capacitive comb structure were rendered. The final optimized layouts are later used to design the masks for the fabrication of the device. It will be covered in detail in the next chapter.

The solid model for the two structures is shown in figure 4.1. The boundary conditions used to simulate strain is indicated in the figures. The bottom face of the substrate was fixed along the Z direction. This is valid as the bottom surface will be attached to the structure under observation for strain measurements. Load patches are defined on either sides of the substrate to apply positive load for simulating compressive strain and negative load for simulating tensile strain. Also all connected surfaces are linked explicitly.

30
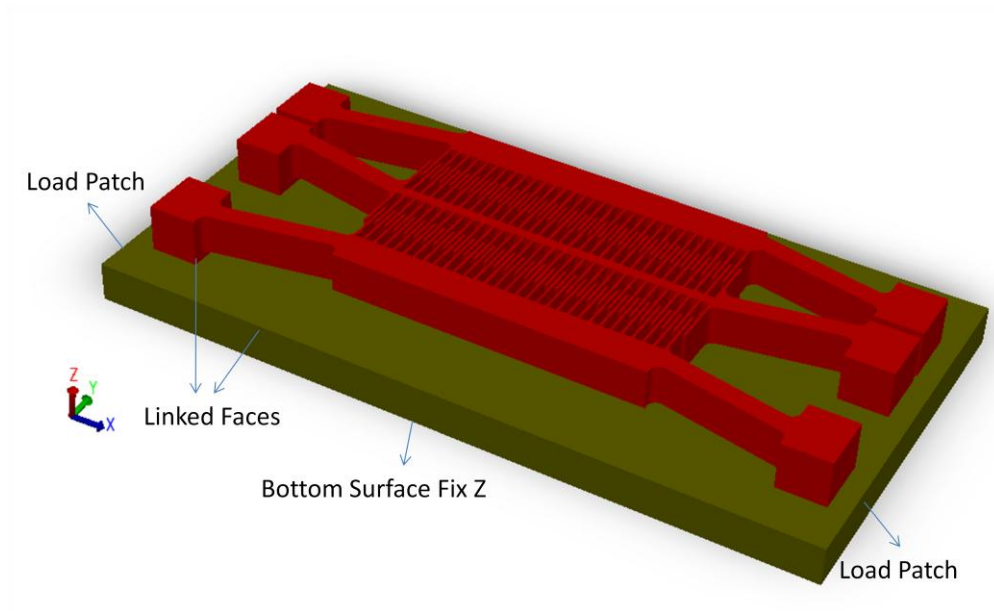
(a)
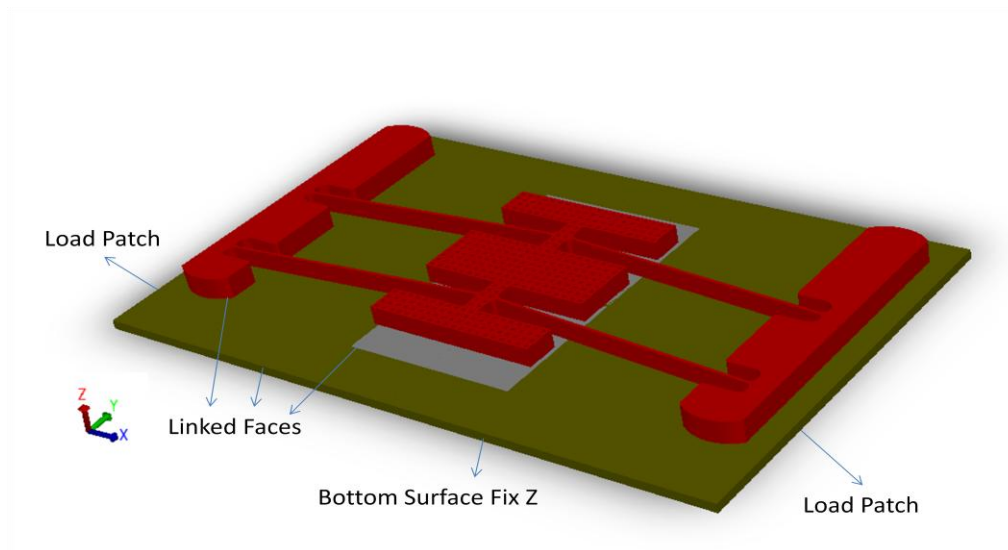
(b)

Figure 4.1 (a) Capacitive Comb Strain Sensor Model with Associated Boundary Conditions (b) Capacitive Plate Strain Sensor Model with Associated Boundary Conditions

4.3.1 Simulations to Study Effect of Beam Width

The plate structure design involved optimization of beam dimensions, plate size, beam position and angle. Initially in an attempt to make the sensor compact the beam length was kept as small as possible. However it was observed that unlike the comb structure the plate structure did not deflect in the Y direction. Instead it exhibited an out of plane bending. This implied that the beam stiffness in the Y direction was much greater than in the Z direction. Simulations were then carried out by systematically varying the different beam parameters. Initially the beam width was reduced in an attempt to reduce the spring constant along the Y direction. However the beam simply bent for moderate strain and this caused a significant reduction in plate displacement. The plate displacement for different beam widths is tabulated in the table below. The stiffness of the beam in the direction of displacement is inversely proportional to its width. However small beam width, the beams are not stiff enough to resist bending and this results in very low net displacement. The results were in agreement with theoretical values derived earlier for beam widths of 10µm or more.

Table 4.2 Effect of Beam Width on Displacement

Beam Width (µm)	Plate Displacement (µm)
5	10
10	38
15	35
20	29

4.3.2 Simulations to study effect of beam height

While deciding the beam height two constraints had to be satisfied. The beam height should be such that the beam stiffness in the Y direction should be less than that in the Z direction. This will ensure that the beam translates in the Y direction on application of strain. Also from fabrication point of view the large beam height would imply high aspect ratio fabrication, which might make it difficult to realize the sensor. Simulation was carried out for different beam heights. As expected the beam height did not have a significant effect on the plate displacement in the Y direction. This was expected from the beam equations seen in the earlier sections.

However if the ratio of beam height to beam width was less than one, the plate would move along the Z axis as opposed to the desired Y direction. The results of the simulation are tabulated in the table below.

Table 4.3 Effect of Beam Height on Plate Displacement

Beam Width(µm)	Beam Height(µm)	Plate Displacement(µm)
10	10	38
10	15	35
10	20	33

4.3.2 Simulations to Study Effect of Beam Length

The length of the beams is the most important and critical design parameter for both the designs. If the length is too short the beams are extremely rigid and do not buckle. On the other hand if the beam length is disproportionately long with respect to the other design parameters it simply bends on application of strain. An additional constrain is placed by the large stress developed in the beam while measuring applied strain. A detailed discussion on stress simulation results, for different beam lengths is discussed later in section 4.3.4.

4.3.3 Simulations to Study Effect of Beam Angle

Another design aspect that was investigated using simulations was the effect of the beam angle on the mechanical gain of the sensor. While the effect of angle of beams on gain for buckled beam structure has been investigated for small strains, the effect of large strains has not been reported. An analytical solution has been reported using the approximation of negligible change in angle of beam due to deflection, however this is not valid for large deflection case where angle of beams change significantly due to beam deflection. MemMech simulation was used to determine effect of angle of beam in the large deflection case. Different models were designed with different beam inclinations and simulated to determine effect of beam angle on displacement gain. The results of the simulation are summarized in table below. While the

33

results follow a trend similar to that reported in case of small linear deflection. However the gain is much less and the increase in gain is not as sharp as in the linear case.

Table 4.4 Effect of Beam Angle on Plate Displacement

Angle (Degree)	Displacement (µm)
5	48
7	43
9	38
11	33

4.3.4 Simulations for Spring Constant Calculation

The spring constant of the beam gives a measure of the flexibility of the beam. While the basic buckled beam operation requires a measure of stiffness, the large displacement requires flexibility to ensure that the stress does not exceed the yield value. Spring constant was measured both directly and indirectly using MemMech simulation. Both the plate and comb structure are suspended by four beams. The SpringMM module was used to find the spring constant of a single beam. The meshed model along with the boundary conditions used is given in the figure below. The actual spring constant of the suspended structure is then found out by simply recognizing the fact that the four springs are in parallel and that the resultant is given by adding the spring constants due to the respective arms.

An alternate method to calculate the spring constant is used to validate the value obtained above. The mass of the sensor is found out in CoventorWare. A known acceleration (1g) is then applied to the sensor. The resultant displacement of the sensor is noted. The following relationship between force F, displacement x, and spring constant K is then used to compute the effective spring constant of the structure.

$$F = kx = mg \tag{4.5}$$

Where, k is the effective spring constant of the structure, m is the mass of the structure and g is the acceleration due to gravity. The resultant spring constant was found to be in agreement with the value obtained above.
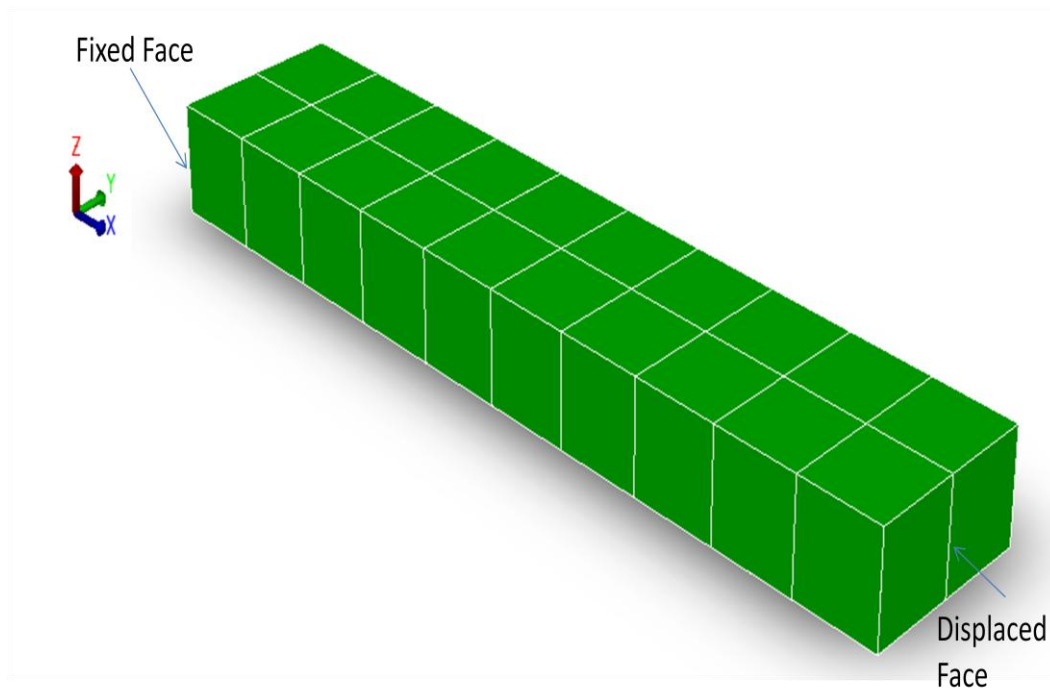
Figure 4.2 Meshed Model and Associated Boundary Conditions used to Measure Spring Constant of Beam
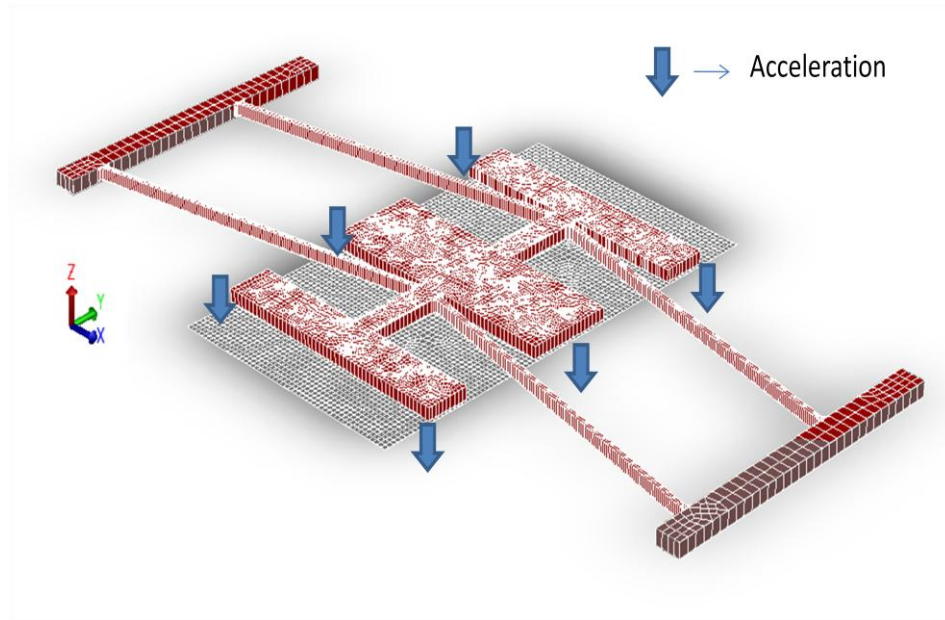
Figure 4.3 Meshed Model used to Measure Spring Constant of Full Structure

4.3.5 Simulations for Optimizing Stress

One of the major concerns while designing the sensor was the high stresses generated in the arm of the sensor due to the large deflection. The different parameters of the arms like width, height, length and material was initially designed to ensure device operation. The device dimension was also kept to the minimum to ensure good compliant characteristics. These design parameters had to be tweaked to ensure that the local stress in the arms is less than the yield stress for the material. The effect of different parameters on stress levels was evaluated and for the given design constrains, the length of the arm was determined to have the most significant effect on the stress.

The stress developed in the arms is highly dependent on the elastic properties of the material. The modulus of elasticity can vary between 170Gpa – 220GPa with corresponding yield strength between 450MPa to 990MPa. FEM simulations were carried out to analyze the effect of beam length on stress. The size of the structure and the large non linear deformation involved required complex meshing techniques. Symmetry condition was used to reduce

36

computational resource requirements. Also it was necessary split the critical parts of the design like the arms from relatively simple parts like anchor and plate to enable finer meshing. The final meshed structure is shown in figure 4.4.The stress was measured along the length of the arm. The data points probed for stress is indicated in the figure 4.5. As expected the stress was found to vary inversely with length. The results indicate that arm lengths varying from 600μm to 800μm is sufficient to maintain stress below yield levels for strain measurements of 0.5% to 3%.

In case of the comb sensor the maximum deflection is limited by the length of the comb fingers and the initial overlap area. An arm length of around 600μm gave a peak local stress of 600MPa for the comb structure. However the plate sensor does not suffer any such constrains and the limiting factor is the yield stress in the arms. By appropriately tuning the length (500μm to 800μm) and width (5μm to 10μm) of the arms sensors were designed to measure strains from 0.5% to 3%. The stress along the length of the arm on application of maximum measurable strain is given in the figure below.
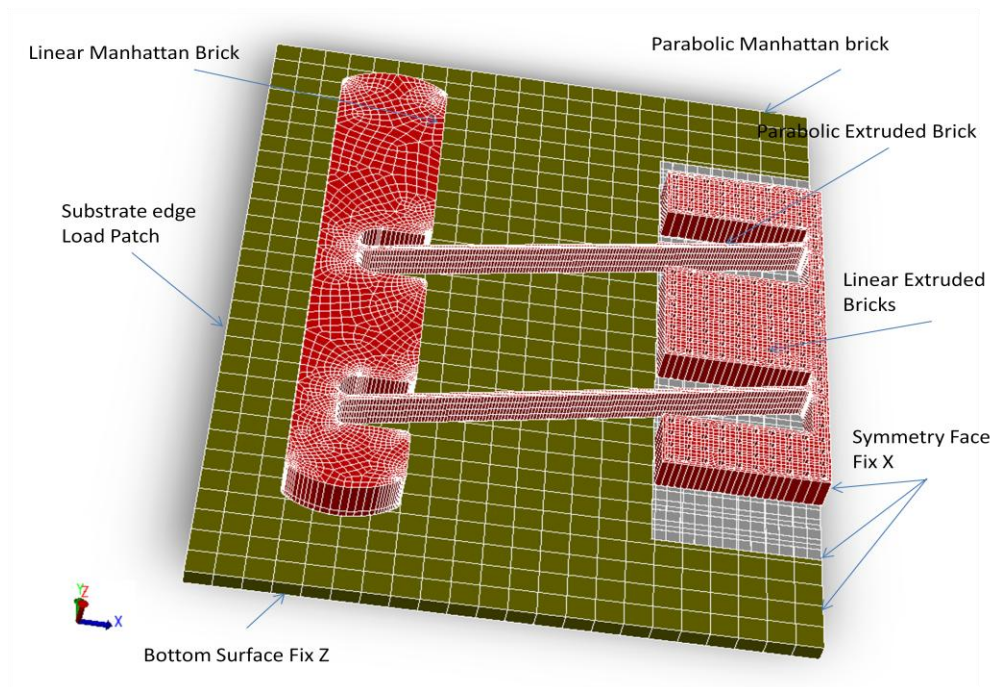
Figure 4.4 Optimized Meshed Structure indicating Mesh Type and Boundary Conditions
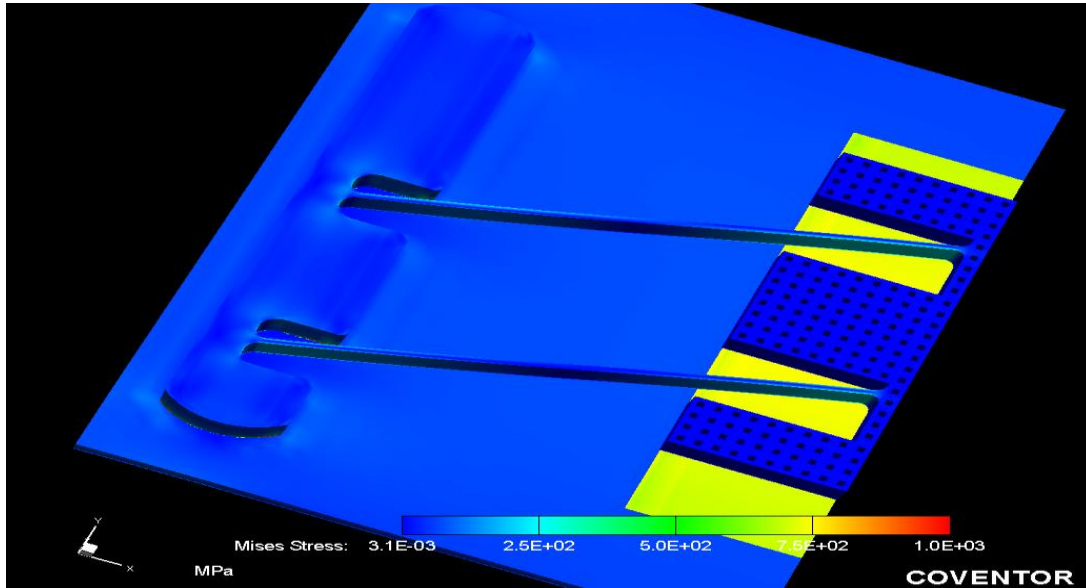
(a)
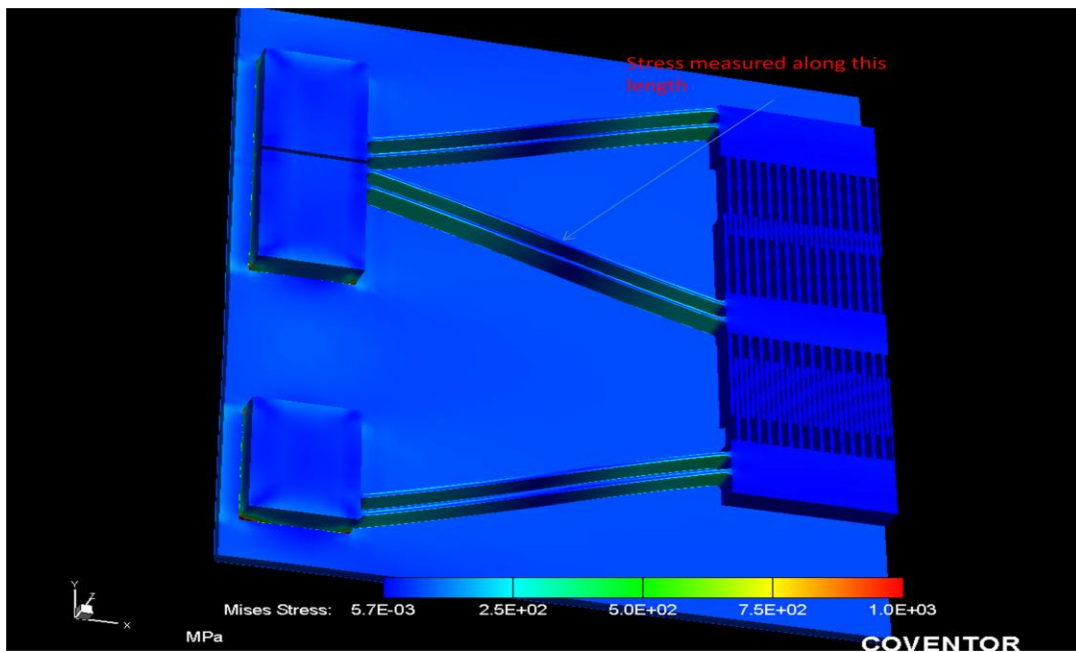
(b)

Figure 4.5 Simulation Result for the Stress Analysis of the Arms for (a) The Comb Structure, (b) The Plate Structure Indicating Points Probed to Obtain Stress Values
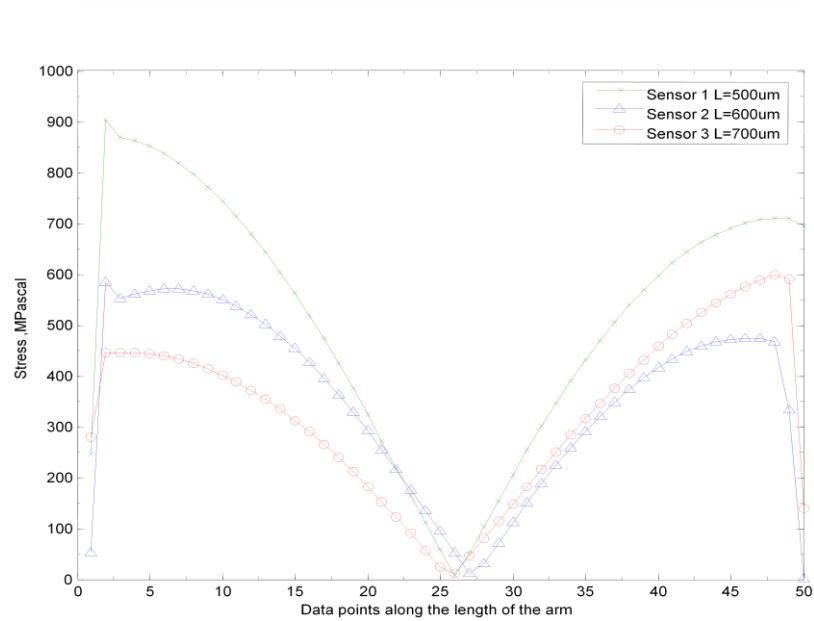
Figure 4.6 Stress along the Length of the Arm for 2% strain for Comb Sensors with Different Arm Lengths.
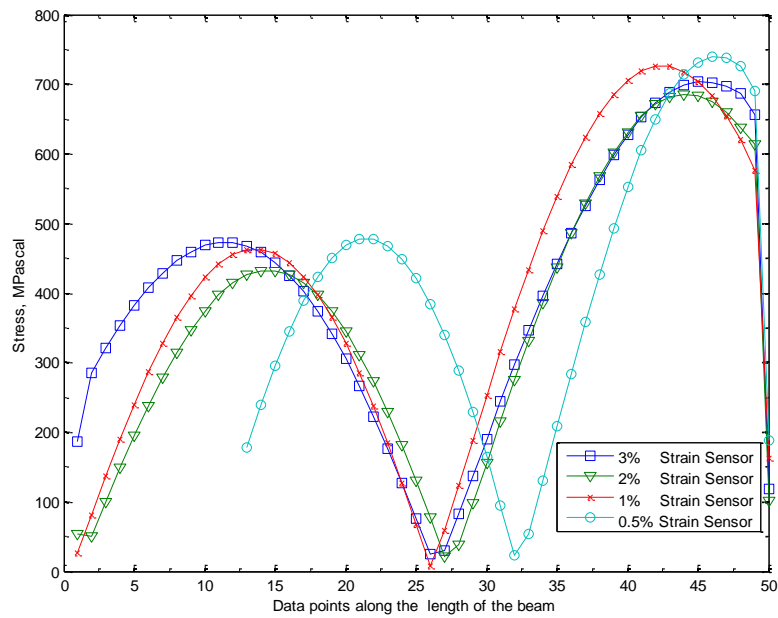
Figure 4.7 Stresses along the Length of the Beam for Different Plate Sensor Designs.

4.3.6 Simulation of Sensor under Varying Strain

The plate displacement due to applied strain is analyzed in CoventorWare, using parametric techniques. The strain condition is simulated by using load patch on the sides of the polyimide substrate as indicated in figure 4.4 earlier. A positive load compress's the substrate, simulating sensor behavior under compressive strain. Likewise a negative load stretches the substrate, simulating tensile strain. It was expected that devices that work for lower strain would not necessarily work for higher strain. On the other hand designing for just high strains reduces the sensitivity at lower strain. Hence the designs were subjected to parametric testing to characterize the device over the entire operating range of the device. These results were then used to select the best devices for different strain measurement range. A parametric simulation was used to apply different loads to the sensor and corresponding strain in the substrate and device behavior was studied.

In MemMech, the Parametric Study function can be used to assign a trajectory to the variable and produce an iterative simulation. Effectively for each step in the trajectory, the simulator solves the problem and generates corresponding results. Thus for a single trajectory, if there are N values, then there will be N simulations are performed. A trajectory simply describes a set of input parameters used to control a study of changing conditions for simulation. A number of parameters can be changed in a systematic manner using different trajectory options available in CoventorWare, such as boundary conditions, material properties and transforms. Up to three trajectories may be set to control the simulations. Table 4.5 and 4.6 below gives the load applied, corresponding strain in substrate and resultant displacement of the structure.

Table 4.5 Load, Strain and Displacement obtained for Comb Sensor

Load	0.5% Strain sensor		1% Strain sensor		2% Strain sensor	
	Strain	Displacement	Strain	Displacement	Strain	Displacement
MPa	%	(µm)	%	(µm)	%	(µm)
0	0	0	0	0	0	0
25	0.29	21.19	0.30	21.21	0.31	18.48
50	0.59	41.33	0.61	41.35	0.63	36.11
75	0.89	60.44	0.93	60.40	0.94	52.95
100	1.19	78.57	1.24	78.42	1.26	69.02
			1.56	95.47	1.58	84.36
			1.87	111.61	1.89	99.03
					2.21	113.07

Table 4.6 Load, Strain, and Displacement Obtained for Plate Sensor

Load	0.5% Strain sensor		1% Strain sensor		2% Strain sensor		3% Strain sensor	
	Strain	Displ.*	Strain	Displ.*	Strain	Displ.*	Strain	Displ.*
MPa	%	(µm)	%	(µm)	%	(µm)	%	(µm)
0	0	0	0	0	0	0	0	0
25	0.29	17.41	0.62	21.55	0.3	10.66	0.30	7.81
50	0.59	33.77	1.25	40.67	0.59	20.75	0.60	15.30
75			1.88	57.27	0.88	30.30	0.89	22.50
100					1.19	39.32	1.19	29.43
125					1.49	47.83	1.49	36.10
150					1.77	55.80	1.79	42.55

Table 4.6 - continued

175					2.06	63.11		
							2.08	48.77
200								
							2.38	54.79
225								
							2.67	60.63
250								
							2.96	66.29

*Disp=>Displacement

4.4 Electrical Simulation

4.4.1. Capacitance

The MemElectro module was used to calculate the capacitance of the structures. MemElectro, which can compute a matrix of capacitance and conductance values or can compute, forces on conductors and dielectrics for MEMS designs. The relationship between charge and voltage for a two-terminal capacitor is defined as

$$Q = C\ (V_1 - V_2)$$

In CoventorWare, MemElectro computes the nodal capacitance matrix, which relates the voltage on the circuit nodes to which the capacitor is connected to the charges on those nodes.

$$\begin{bmatrix} q_1 \\ q_2 \end{bmatrix} = \begin{bmatrix} C & -C \\ -C & C \end{bmatrix} \begin{bmatrix} V_1 \\ V_2 \end{bmatrix}$$

Where,

$q_1 = -q_2 = Q$ is the charge stored in the matrix,

C is the capacitance of the device

V_1 and V_2 are the voltages of the nodes.

4.4.1.1 Capacitance of plate structure

The plate structure was also simulated using MemElectro for capacitance measurement. Extruded parabolic mesh (X = 10um, Y =10um, Z= 10um) was used for the

42

mesh. The meshed structure is shown below. The capacitance matrix obtained for the plate structure is

$$C_{(d=2)} = \begin{bmatrix} 0.5284 & -0.0054 & -0.5229 \\ -0.0054 & 0.5285 & -0.5231 \\ -0.5229 & -0.5231 & 1.0461 \end{bmatrix}$$

The capacitance value is in Pico-Farads. The first two diagonal elements are the capacitance between the bottom plates and the top plate. The capacitance of the plate structure with a gap of 4µm was found to be 0.276pF per capacitor and 0.5284pF for a gap of 2 µm. The capacitance value obtained is in reasonable agreement with theoretical values. The slight increase in capacitance value can be accounted by the fringe field.

4.4.1.2 Capacitance of Comb Structure

The comb structure was meshed using Manhattan Bricks (X = 10um, Y =10um, Z=20um). The meshed structure is shown in figure below. The advanced setting tab was tweaked to ensure the convergence of the result. The rest capacitance of the sensors varies between 586fF to 1068fF for finger separation of 3µm to 2µm respectively.

4.4.2. Pull in Voltage

The pull in voltage optimization is extremely critical for the design. The large size of the device makes it both very sensitive to pull-in and difficult to simulate. The length of the arm L, the beam width B, height H and plate separation D are the primary variables that control the pull-in. The spring constant and capacitance values obtained from the mechanical and electrical simulations of the structure were used to find the pull in voltages for the plate based strain sensors. A bias voltage of 2.5 to 5 volts will be applied to the device. The pull in voltage should be tuned to at least four times this value to ensure proper operation. Table 4.7 gives the pull-in voltages for select devices.

Table 4.7 Pull-in Voltage Obtained for Selected Designs.

L(μm)	B(μm)	H(μm)	D(μm)	K_{mz}	$V_{pull-in}$(V)
800	10	10	4	15.88	11.4
800	10	20	4	125	31.92
800	10	20	2	125	22.56
700	10	20	4	185.6	39.04
700	10	20	2	185.6	27.61
600	10	20	4	296.28	49.22
600	10	20	2	296.28	34.8
600	5	20	4	148.16	34.8
600	5	20	2	148.16	24.61

CHAPTER 5

FABRICATION OUTLINE

The structure has to measure very high strain and hence the process is carefully formulated to ensure minimum micro defects in the different layers. Small cracks or high local residual stress regions can act as initiation points for fracture or inelastic expansion. Also different deposition processes have to be optimized to ensure small grain size to ensure high strength [39].

Fabrication ease and repeatability was one of the primary considerations of the design. The objective was to ensure a design and fabrication process that allows good fabrication tolerance, relaxed constraint on the equipment, high repeatability and relatively inexpensive fabrication.

Mask was designed for both the designs. While the simulation results indicate a good agreement with desired specification the fabrication has to be carefully planned and executed to realize the device. Fabrication of the sensor will involve wafer cleaning, spin coating, photo lithography, film deposition, lift-off and electro-deposition. The proposed fabrication steps are described in detail along with specific requirements and reasoning for the selected processes. Fabrication is carried out on a 4 inch 100 silicon wafer. Surface micromachining is used exclusively used for the fabrication. Surface micromachining is essentially the deposition, patterning, and etching of a sequence of thin films with thickness varying between a few 100nm to a 100µm.

5.1 Masks

The mask was designed in CoventorWare Designer. Several designs were selected and optimized for different strain and sensitivity levels. Since both designs follow almost identical processing steps, all the variations of both the designs were included in the same die. The OAI Backside Contact Aligner has a minimum feature 1µm and care is taken to ensure feature sizes are larger than this. Figure 5.1 shows the mask designed for the different layers.

45
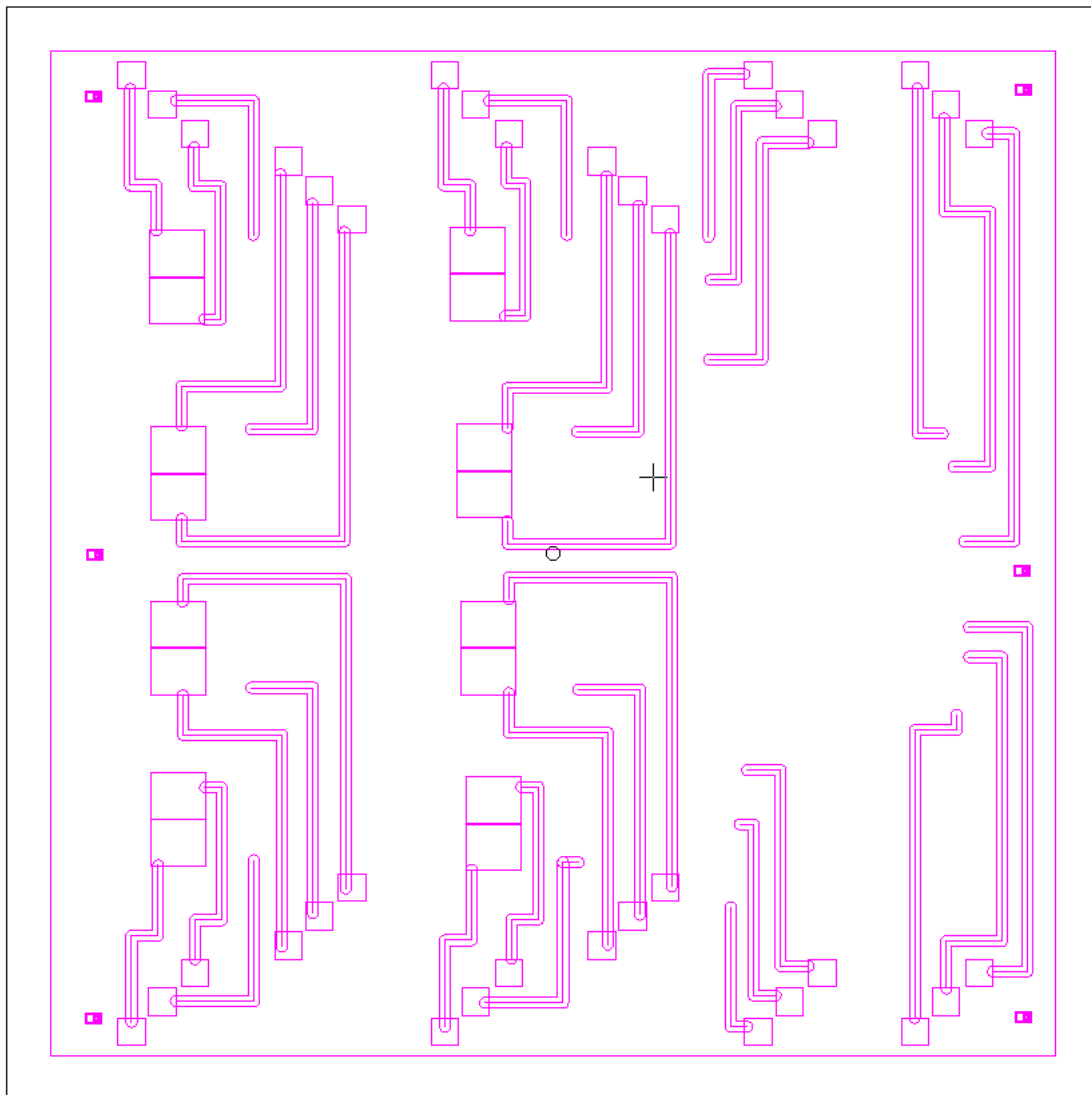
Figure 5.1 Mask for Metallization Layer

Figure 5.2 Mask for Anchor

Figure 5.3 Mask for Seed Layer

5.2 Process Flow
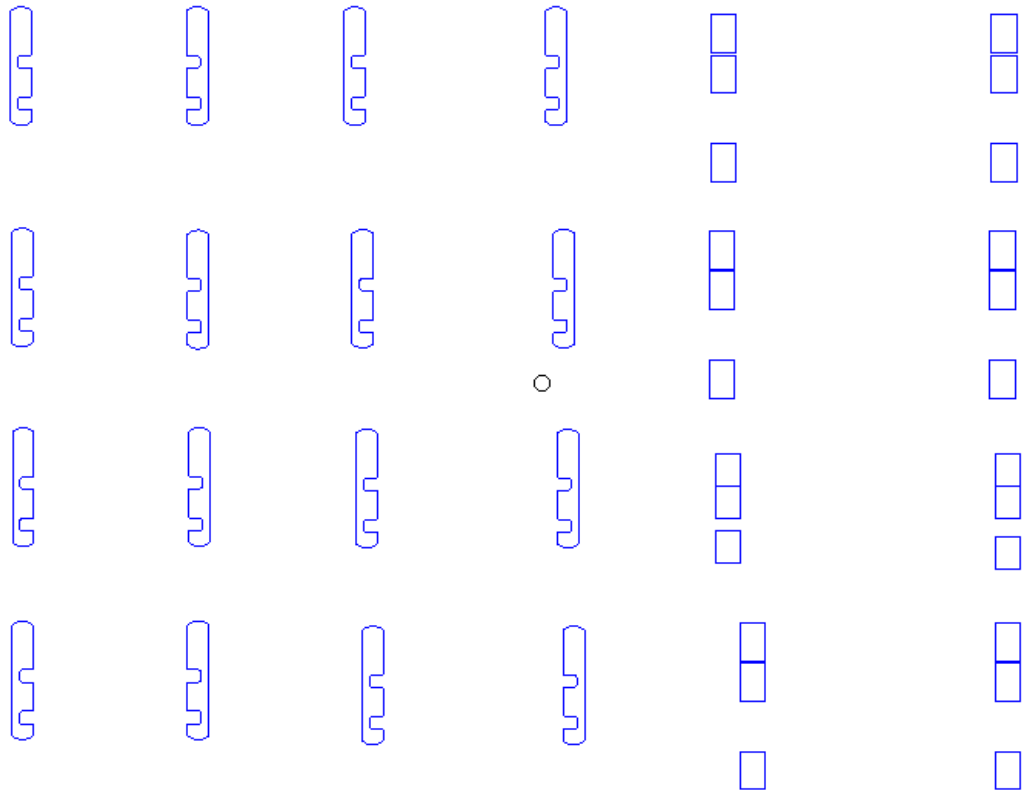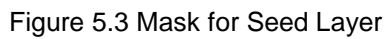
The device fabrication steps are illustrated in figure 5.2. The fabrication of the comb sensor is similar with a few exceptions. There is no need for a bottom electrode, although a metallization layer step is required. Also the combs will decide the minimum feature size for the comb based sensor.

(a) Deposit Nitride Layer

(b) Spin Coat Polyimide

(c) Deposit Metallization Layer

(d) Deposit Protective Oxide Layer

(e) Spin Coat Sacrificial Polyimide

(f) Deposit Titanium and Seed Gold Layer

(g) Spin Coat Mold Photo Resist

(h) Electroplate Nickel and Remove Mold

(i) Remove Sacrificial, Oxide and Seed Layer

Silicon   PI2611   HD4104   NR4800P Neg. Resist

Silicon Oxide   Aluminium   Titanium/Gold   Nickel

Figure 5.4 Fabrication Steps for the Plate and Comb Structures.

5.3 Wafer Cleaning

The wafer is first immersed in TCE for 5 minutes to degrease it. It is then immersed in acetone for 3 minutes. This removes the TCE residue and acts as a further cleaning solvent. The residue due to the previous step is then removed by immersing it in methanol for 3 minutes. The wafer is then rinsed in running DI water for 3 minutes. RCA standard clean 1 (base piranha or piranha) is then used to remove insoluble organic contaminants. The wafer is immersed in a hot mixture (75 C) of water-diluted hydrogen peroxide and ammonium hydroxide (5:1:1 $H_2O:H_2O_2:NH_4OH$) for 10 min. This removes organic surface films by oxidative breakdown and dissolution to expose the silicon or oxide surface for concurrent or subsequent decontamination

49

reactions. Group IB and IIB metals and several other metals, including gold, silver, copper, nickel, cadmium, zinc, cobalt, and chromium, are dissolved and removed by the complexing effectiveness of ammonium hydroxide; copper, for example, forms the $Cu(NH^3)^4$ & amino-complex. Higher temperatures must be avoided to minimize excessive thermal decomposition of the hydrogen peroxide. The above mixture is sometimes called Base-Piranah. It can be used to remove light organics. For heavy contaminations instead of it Piranha solution, a mixture of sulfuric acid and hydrogen peroxide can be used. It is a strong oxidizer and it will remove most organic matter and it will also hydroxylate most surfaces (adds OH groups), making them extremely hydrophilic. Any metallic contaminants may have accumulated as a result of organic clean in the thin oxide layer is removed with a 50:1 H^2O:HF solution for 15 secs. An oxide removal step tends to add particles to wafer surface it is often followed by a NH^40H /H^2O^2 step.Particles are removed by slow etching the silicon from under the surface of metal particles.It also passivates the surface by forming a thin oxide layer on the wafer effectively making it hydrophilic. Ionic and heavy metal atomic contaminants using a hot mixture of water-diluted hydrogen peroxide and hydrochloric acid (6:1:1 H^2O:H^2O^2: HCl).This procedure was designed to remove alkali ions, and cations such as Al, Fe and Mg that form NH^4OH-insoluble hydroxides in basic solutions. This also eliminates metallic contaminants that were not entirely removed by the first treatment, such as gold, nickel, cobalt, copper, lead and aluminium. Electrochemical displacement replating of heavy metals from the solution is prevented by formation of soluble complexes with the dissolved metal ions.

5.4 Silicon Nitride Deposition

Silicon Nitride is commonly deposited by reacting silicon contacting gases and ammonia.

$3SiCl_2H_2 + 4NH3 \rightarrow Si_3N_4 + 6HCL + 6H_2$

50
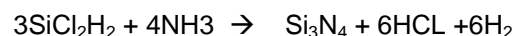
PECVD nitride is often non-stoichiometric i.e. the ratio of silicon, nitrogen and hydrogen in it, is not fixed. It has high concentrations of hydrogen and large residual stress. However, the stress level can adjusted by tuning the RF frequency during deposition. A nitride film deposited at 13.5Mhz has a residual stress of 400MPa (tensile), while a film deposited at 50Khz has a stress of 200MPa (compressive). Also as reactor pressure is reduced stress changes form tensile to compressive. One of the major drawbacks of PECVD nitride is that it has a high HF etch rate often greater than silicon oxide.

LPCVD is used to deposit a stoichometric silicon nitride film. Typical deposition temperatures range from 500 C to 700 C at a pressure of 200mtorr to 500mtorr. LPCVD nitride has high residual tensile strength, up to 10^{10} dynes/cm^2. A LPCVD nitride film of thickness more than a few 1000 Angstroms will simply crack. The film stress can be adjusted by increasing the silicon content of the film. This is typically done by using dichlorosilane in higher proportion. A nearly stress free film can be grown by using a dichlorosilan ammonia ratio of 6:1, at 850 degree Celsius temperature and 500mTorr pressure. LPCVD nitride has good HF etch resistance. LPCVD nitride is deposited at these optimized conditions for device fabrication [40-42] .

<center>5.5 Substrate Polyimide</center>

The flexible substrate will be made of polyimide. Since it will be subjected to significant strain low stress polyimide PI2611 is selected for the flexible substrate. PI2611 is obtained from HD Microsystems, as a polyamic acid precursor dissolved in an n-methyl-2-pyrrolidone (NMP) based solvent. This can be spin coated on the substrate and then thermally cured to obtain the polyimide film.

The precursor is first spin coated on the substrate. It is first dispensed manually on a clean Silicon wafer. It is spread at 500rpm for 5 seconds to uniformly distribute it over the wafer. It is then spun at 2000rpm for 30 seconds. This is followed by a Pre-Soft bake at room temperature for 30 minutes. It is then heated to 90 °C for 90 seconds on a hot plate and then at the same temperature in a convection oven for 7 minutes. Soft bake is carried out first, at 150 °C for 90

<center>51</center>

seconds on a hot plate and then at 120 °C for 3 minutes in a convection oven. Hard bake is done over 350 °C in a nitrogen environment in the oven. A ramp speed of 2 °C/min is used for ramping the temperature while increasing and decreasing it. The hotplate is used at each stage to ensure that air bubbles do not get trapped in the polyimide, and is them followed by heating in convection oven to ensure uniform heating and provide a nitrogen environment. Polyimide layers approximately 8μm thick can be obtained in this fashion.

A 50μm thick polyimide substrate is required. Several layers of polyimide will have to be used to achieve this. The above process is repeated two times with the final cure temperature of 170 °C. The third layer is then deposited and processed with a final cure temperature above 400 °C. The first two steps are again repeated followed by the last deposition step which will have a final curing temperature above 350 °C [43].

5.6 Metallization

Liftoff is used to pattern the metallization layer. A protective oxide layer is first deposited using ion beam sputtering and anchor windows are opened in it. NR-9 1500 PY (Futurrex) negative photoresist is spin-coated and patterned using the metallization mask. The exposed polyimide is treated with oxygen plasma in a reactive ion etcher at 120W for 1 minute to improve adhesion of the metallization layer. 50 angstroms of titanium is then deposited at room temperature in an AJA ATC Orion series E-beam Evaporator. This is followed by sputter deposition of a 0.5μm Al layer. Acetone is used to strip of the photo resist to form the bottom electrodes, interconnect wires and contact pad.

5.7 Nickle Deposition

An oxide layer is then deposited using ion beam sputtering and anchor windows are opened in it. Since subsequently a polyimide sacrificial is used. A protective layer is required to prevent etching of the polyimide substrate. However this layer has to be eventually removed as it will not be able to survive high strain values that it will be subjected to during strain measurements. Silicon oxide can be easily removed as opposed to silicon nitride, hence the choice. The oxide

layer is then deposited using ion beam sputtering and anchor windows are opened in it using liftoff.

A sacrificial layer of photo-definable polyimide (HD4104) is then spin coated, patterned and developed to open windows for the anchor. The precursor is manually dispensed and then spread at 500rpm for 5 seconds to uniformly distribute it over the wafer. It is then spun at 3500rpm for 30 seconds. This is followed by a Pre-Soft bake at room temperature for 30 minutes. It is then heated to 90 °C for 100 seconds on a hot plate and then at 100 °C temperature in a convection oven for 100 seconds. Soft bake is carried out at 200 C for 30 minutes in a convection oven. Hard bake is done at 375 °C in a nitrogen environment in the oven for 60 minutes. A ramp speed of 2 °C/min is used for ramping the temperature while increasing and decreasing it.   This approximately gives a 3μm film. The polyimide is then treated with oxygen plasma and an intermediate adhesion layer of titanium is deposited in the e beam evaporator. 1000 Å thick gold seed layer is then deposited at room temperature using e-beam evaporator. A 20μm thick NR-4 8000P negative photo resist layer is then spin coated and patterned to make a mold for electro deposition.

A custom electroplating setup previously developed in our group is used. Electroplating is done in a nickel sulphamate solution which was circulating in the plating tank at a rate of 6 gallons/minute. Nickel sulphamate was preferred due to its low stress and high deposition rate compared with Watts solutions. A current density of 2mA/cm^2 at 45 °C is used.

A low current density (2mA/cm^2) is required to ensure that high quality, high yield strength nickel is obtained. The mold resist is removed in acetone. Standard gold etch solution of KI: I_2:H_2O (4gm: 1gm: 40ml) is used to etch the gold seed layer. Oxygen plasma etching is then used to remove the sacrificial polyimide and release the plate structure. Buffered oxide etch is finally used to remove the passivating silicon oxide layer. The wafer is then diced to separate the device and immersed in water to release the polyimide layer from the silicon wafer.

CHAPTER 6

CONCLUSION AND FUTURE WORK

This thesis describes the initial development of a capacitive strain sensor. A simple design approach was utilized to realize a capacitive strain sensor to measure large strain. Basic beam equations were used to design an approximate structure which was then optimized using Finite element method simulations. Two different topologies a comb based structure and a parallel plate based structure. While the former has been reported before, it was only designed for small strains, less than 1000uε. The latter is a completely new design and is superior in several ways.

The variation in capacitance due to the applied strain for devices optimized for different strains is given in figure6.1 and 6.2. The gauge factor for a capacitive strain sensor is defined by equation 5.1.

$$Gauge\ Factor = \frac{\Delta C/_C}{\varepsilon} \qquad\qquad (6.1)$$

Table 6.1 gives the gauge factor obtained for the different designs. The comb and plate structures were both designed for approximately equal rest capacitance. The gauge factor for the 2% strain sensors was 51.72 compared to 38.24 obtained for the plate sensor. However unlike the plate structure where the yield stress limits the maximum measureable strain, the finger length and overlap area limits the maximum measureable strain in the comb topology.

The yield stress limits the maximum measurable tensile strain to 2%. A strain with a random orientation might result in shorting of the combs especially for large strains. The topology of the comb sensor does not allow any sort of compacting and the device is 75% larger than the

54

capacitive plate structure. Also despite the larger size the comb device optimized for high operating range could measure only up to 2% strain. Nonlinearity is expected in the comb structure
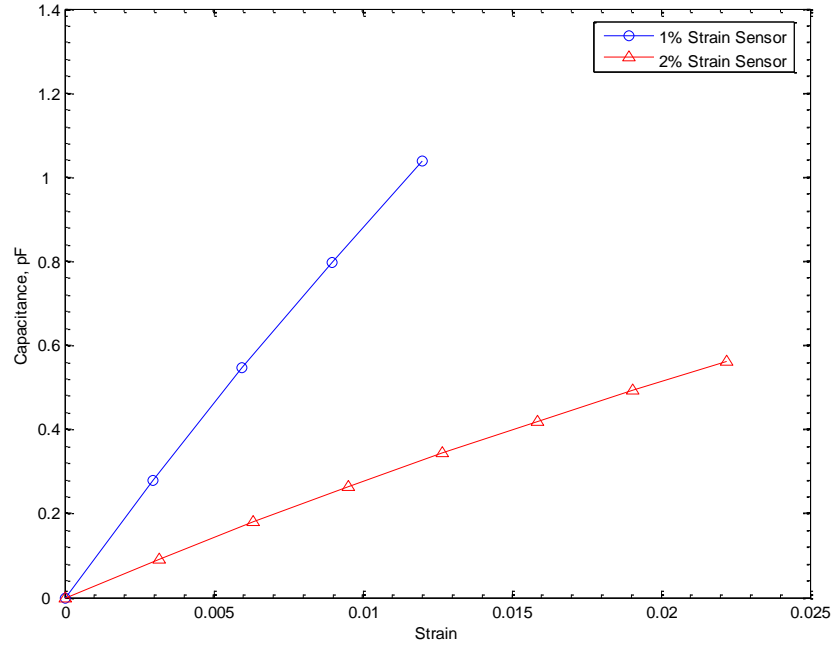

Figure 6.1 Differential Capacitance Obtained for Different Applied Strain for the Comb Structure.

towards the maximum measurable strain due to the additional capacitance between the finger edge of the central conductor and the outer electrode, this is not the case for the plate structure. The sensors have been designed for a flexible substrate which allows conformal attachment to different surfaces. It is expected that, the flexibility of the structures whose strain has to be measured, is much less than polyimide, hence maximum strain will be transferred to the sensors. The fabrication of the comb structure requires high aspect ratio (10:1) as compared to the plate sensor (2:1). Some key aspects of the design need further investigation. The device has demonstrated a higher stress level for tensile strain as compared to the compressive case. The final die mask includes interconnect wires and bond pads. While these have been designed

to withstand the large strain it would be prudent to encapsulate them inside the polymer. The
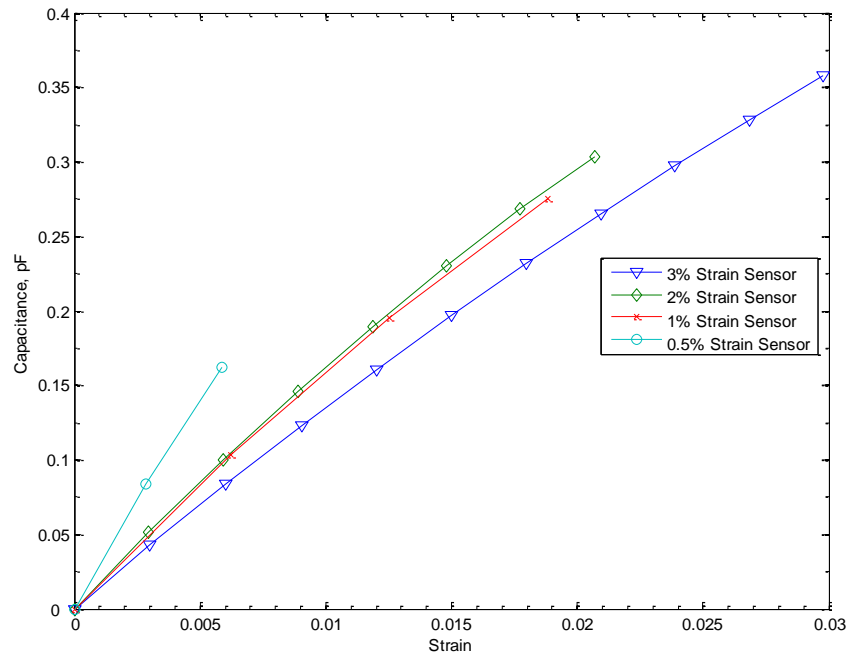

Figure 6.2 Differential Capacitance Obtained for Different Applied Strain for the Plate Structure.

Table 6.1 Gauge Factor Obtained for Different Sensors.

Capacitive Plate Sensor	Gauge Factor	Capacitive Comb Sensor	Gauge Factor
3% Strain Sensor	19.12	2% Strain Sensor	51.72
2% Strain Sensor	38.24	1% Strain Sensor	85
1% Strain Sensor	38.24		
0.5% Strain Sensor	57.36		

packaging of the device is also challenging due to the vertical profile of the device and the large

strain levels involved. A packaging scheme has to be developed for this sensor.

In conclusion the capacitive plate based sensor is ideal for measuring large strain with high

sensitivity. The design can be optimized for higher sensitivity but lower range to measure

smaller strains. The comb based sensor has a higher sensitivity as compared to the plate based

design for a given strain but cannot measure as high a strain.

REFERENCES

[1]   G. Bartelds, "Aircraft structural health monitoring, prospects for smart solutions from a European viewpoint," *Structural Health Monitoring. Current Status and Perspectives,* pp. 18–20, 1998.

[2]   D. Pines and A. Aktan, "Status of structural health monitoring of long span bridges in the United States," *Progress in Structural Engineering and materials,* vol. 4, pp. 372-380, 2002.

[3]   C. Farrar and K. Worden, "An introduction to structural health monitoring," *Philosophical Transactions of the Royal Society A: Mathematical, Physical and Engineering Sciences,* vol. 365, p. 303, 2007.

[4]   A. Raghavan and C. Cesnik, "Review of guided-wave structural health monitoring," *Shock and Vibration Digest,* vol. 39, pp. 91-116, 2007.

[5]   M. Reda Taha and J. Lucero, "Damage identification for structural health monitoring using fuzzy pattern recognition," *Engineering Structures,* vol. 27, pp. 1774-1783, 2005.

[6]   E. Sazonov*, et al.*, "Signal processing and power issues in acquisition of vibration data by MEMS accelerometers," *Sigma,* vol. 24, p. 780.

[7]   C. Farrar*, et al.*, "Vibration–based structural damage identification," *Philosophical Transactions A,* vol. 359, p. 131, 2001.

[8]   M. Bement and C. Farrar, "Issues for the application of statistical models in damage detection," 2000.

[9]   C. Byington*, et al.*, "Prognostic enhancements to diagnostic systems for improved condition-based maintenance," 2002.

[10]   K. Bethe, "The scope of the strain gage principle," 2002, p. 3.

[11]   Y. Kanda, "A graphical representation of the piezoresistance coefficients in silicon," *IEEE Transactions on Electron Devices,* vol. 29, pp. 64-70, 1982.

[12]   M. Hrovat*, et al.*, "An evaluation of some commercial thick film resistor materials for strain gauges," *Journal of Materials Science Letters,* vol. 13, pp. 992-995, 1994.

[13]   A. Window, *Strain gauge technology*: Springer, 1992.

[14]   C. CHO, "Experimental characterization of the temperature dependence of the piezoresistive coefficients of silicon," 2007.

[15]   R. Jaeger*, et al.*, "Thermally induced errors in the calibration and application of silicon piezoresistive stress sensors," *Advances in Electronic Packaging 1993,* pp. 4-1.

[16]   C. Cao*, et al.*, "Temperature dependent piezoresistive effect of multi-walled carbon nanotube films," *Diamond and Related Materials,* vol. 16, pp. 388-392, 2007.

[17]   A. Reale*, et al.*, "Evaluation of the gauge factor for membranes assembled by single-walled carbon nanotubes," *Applied Physics Letters,* vol. 85, p. 2812, 2004.

[18]   R. M. Measures, *Structural monitoring with fiber optic technology*: Academic Press, 2001.

[19]   W. H. Ko*, et al.*, "A high-performance MEMS capacitive strain sensing system," *Sensors and Actuators A: Physical,* vol. 133, pp. 272-277, 2007.

[20]   J. T. Lin*, et al.*, "A high gauge factor capacitive strain sensor and its telemetry application in biomechanics," *2008 17th Biennial University/ Government/ Industry Micro-Nano Symposium, Proceedings,* pp. 98-101, 2008.

[21]   K. Arshak*, et al.*, "Development of new capacitive strain sensors based on thick film polymer and cermet technologies," *Sensors and Actuators A: Physical,* vol. 79, pp. 102-114, 2000.

[22] L. Que*, et al.*, "A micromachined strain sensor with differential capacitive readout," in *Mems '99: Twelfth Ieee International Conference on Micro Electro Mechanical Systems, Technical Digest*, ed New York: Ieee, 1999, pp. 552-557.

[23] R. Matsuzaki and A. Todoroki, "Wireless flexible capacitive sensor based on ultra-flexible epoxy resin for strain measurement of automobile tires," *Sensors and Actuators A: Physical,* vol. 140, pp. 32-42, 2007.

[24] I. Ward and J. Sweeney, *An introduction to the mechanical properties of solid polymers*: John Wiley & Sons Inc, 2004.

[25] W. Chang*, et al.*, "Physical characteristics of polyimide films for flexible sensors," *Applied Physics A: Materials Science & Processing,* vol. 92, pp. 693-701, 2008.

[26] R. Norton, *Machine design: an integrated approach*: Prentice Hall, 2000.

[27] C. Liu, "Recent developments in polymer MEMS," *Advanced Materials,* vol. 19, pp. 3783-3790, 2007.

[28] C. Lee*, et al.*, "Fabrication of micro sensors on a flexible substrate," *Sensors and Actuators A: Physical,* vol. 147, pp. 173-176, 2008.

[29] C. Chen*, et al.*, "An electrohydrodynamic micropump for on-chip fluid pumping on a flexible parylene substrate," 2007, pp. 826-829.

[30] H. D. Microsystems, "Product Selector's Guide," ed.

[31] C. Shih*, et al.*, "Yield strength of thin-film parylene-C," *Microsystem Technologies,* vol. 10, pp. 407-411, 2004.

[32] T. Harder*, et al.*, "Residual stress in thin-film parylene-C," 2002, pp. 435-438.

[33] Paralyene Coating Services Inc, ed.

[34] B. Stark, *MEMS reliability assurance guidelines for space applications*: Citeseer, 1999.

[35] M. Gad-el-Hak, *The MEMS handbook*: CRC, 2006.

[36] D. C. Baek*, et al.*, "Measurement of mechanical properties of electroplated nickel thin film," *Advances in Fracture and Failure Prevention, Pts 1 and 2,* vol. 261-263, pp. 417-422, 2004.

[37] T. Fritz*, et al.*, "Characterization of electroplated nickel," *Microsystem Technologies,* vol. 9, pp. 87-91, 2002.

[38] W. Sharpe Jr*, et al.*, "Measurements of Young's modulus, Poisson's ratio, and tensile strength of polysilicon," 2002, pp. 424-429.

[39] T. Wu and R. Rosler, "Stress in PSG and nitride films as related to film properties and annealing," *Solid state technology,* vol. 35, pp. 65-72, 1992.

[40] M. Madou, *Fundamentals of microfabrication: the science of miniaturization*: CRC, 2002.

[41] B. Bhushan, *Springer handbook of nanotechnology*: Springer Verlag, 2006.

[42] M. Sekimoto*, et al.*, "Silicon nitride single layer x ray mask," *Journal of Vacuum Science and Technology,* vol. 21, pp. 1017-1021, 2009.

[43] P. Xu, "Hybrid X-band power amplifier development for 3D-IC phased array module," 2003.

BIOGRAPHICAL INFORMATION

Clement Jacob was born in Bombay (now Mumbai), India on the 30th of July 1985. He graduated with a Bachelors Degree in Electrical Engineering from Mumbai University, India in May 2007. He joined as a Lecturer and Research Associate in Don Bosco Institute of Technology, DBIT (Affiliated Mumbai University), his alma matter, in June 2007. He instructed undergraduate students in Basic Electrical Engineering and Image Processing at DBIT. He also developed a low power jammer during his time at the institute. He joined the University of Texas at Arlington, in fall 2008 to further his interest in research and academics. He developed a novel capacitive strain sensor for structural health management under the guidance of Dr. Donald Butler. The sensitivity is the highest reported for a device that can measure 30,000µɛ. He aims to pursue research and integrate technologies that can be developed into products which can have an immediate impact on the society.